Long-lived mesoscale eddies in the eastern Mediterranean Sea: Analysis of 20 years of AVISO geostrophic velocities

Nadia Mkhinini, Andre Luis Santi Coimbra, Alexandre Stegner, Thomas Arsouze, Isabelle Taupier-Letage, Karine Béranger

AGU PUBLICATIONS

JGR

Journal of Geophysical Research: Oceans

RESEARCH ARTICLE

10.1002/2014JC010176

Key Points:
- Eddy detection algorithm
- Cyclone anticyclone asymmetry
- Formation of long-lived eddies in the eastern Mediterranean Sea

Correspondence to:
T. Arsouze,
thomas.arsouze@ensta-paristech.fr

Citation:
Mkhinini, N., A. L. S. Coimbra, A. Stegner, T. Arsouze, I. Taupier-Letage, and K. Béranger (2014), Long-lived mesoscale eddies in the eastern Mediterranean Sea: Analysis of 20 years of AVISO geostrophic velocities, *J. Geophys. Res. Oceans*, *119*, 8603–8626, doi:10.1002/2014JC010176.

Received 23 MAY 2014
Accepted 10 NOV 2014
Accepted article online 13 NOV 2014
Published online 16 DEC 2014

Long-lived mesoscale eddies in the eastern Mediterranean Sea: Analysis of 20 years of AVISO geostrophic velocities

Nadia Mkhinini[1,2], Andre Louis Santi Coimbra[2], Alexandre Stegner[1,2], Thomas Arsouze[1,2], Isabelle Taupier-Letage[3], and Karine Béranger[2]

[1]Laboratoire de Météorologie Dynamique, École Polytechnique, Palaiseau, France, [2]UME, ENSTA-ParisTech, Paris, France, [3]Aix Marseille Université, CNRS, Université de Toulon, IRD, MIO UM 110, 13288, Marseille, France

Abstract We analyzed 20 years of AVISO data set to detect and characterize long-lived eddies, which stay coherent more than 6 months, in the eastern Mediterranean Sea. In order to process the coarse gridded ($1/8^{\circ}$) AVISO geostrophic velocity fields, we optimized a geometrical eddy detection algorithm. Our main contribution was to implement a new procedure based on the computation of the Local and Normalized Angular Momentum (LNAM) to identify the positions of the eddy centers and to follow their Lagrangian trajectories. We verify on two mesoscale anticyclones, sampled during the EGYPT campaign in 2006, that our methodology provides a correct estimation of the eddy centers and their characteristic radius corresponding to the maximal tangential velocity. Our analysis reveals the dominance of anticyclones among the long-lived eddies. This cyclone-anticyclone asymmetry appears to be much more pronounced in eastern Mediterranean Sea than in the global ocean. Then we focus our study on the formation areas of long-lived eddies. We confirm that the generations of the Ierapetra and the Pelops anticyclones are recurrent and correlated to the Etesian wind forcing. We also provide some evidence that the smaller cyclonic eddies formed at the southwest of Crete may also be induced by the same wind forcing. On the other hand, the generation of long-lived eddies along the Libyo-Egyptian coast are not correlated to the local wind-stress curl but surprisingly, their initial formation points follow the Herodotus Trough bathymetry. Moreover, we identify a new formation area, not discussed before, along the curved shelf off Benghazi.

1. Introduction

The improved spatial resolution of sea surface fields in the AVISO altimetry merged data revealed the prevalence of mesoscale eddies throughout most of the oceans [*Isern-Fontanet et al.*, 2003, 2006b; *Morrow et al.*, 2004; *Chelton et al.*, 2007, 2011; *Chaigneau et al.*, 2008, 2009]. Among the various methods used to detect and sample surface oceanic eddies from field measurements, the use of sea surface altimetry, which is not affected by cloud coverage, is among the most efficient ways to track long-lived eddies. The recent progress in automated eddy detection algorithms [*Sadarjoen et al.*, 1998; *Isern-Fontanet et al.*, 2003; *Nencioli et al.*, 2010; *Chelton et al.*, 2011] enables to identify the positions of coherent structures and to follow their Lagrangian trajectories during several months. Among the thousands eddies that could be identified at any given time, a small but significant number of long-lived eddies, lasting more than 6 months, were detected in specific regions such as the southeastern Atlantic Ocean [*Schonten et al.*, 2000], the eastern South-Pacific [*Chaigneau et al.*, 2008], or the northeastern subtropical Atlantic [*Sangrà et al.*, 2009]. Moreover, *Chelton et al.* [2011] detected, over 16 years of data record of the global ocean, more than 600 surface eddies with lifetime that exceed 2 years. The presence of such long-lived eddies could strongly impact the surface circulation at both local and regional scale. Indeed, these coherent structures trap and transport heat, mass, momentum, and biogeochemical properties from their regions of formation to remote areas.

In many closed or semiclosed seas, the circulation is dominated by gyres and coastal eddies, and the kinetic energy of the instantaneous eddy field is larger than the kinetic energy of the long-term average circulation. This is the case of the Mediterranean Sea, which exhibits a complex circulation system [*Millot and Taupier-Letage*, 2005; *Isern-Fontanet et al.*, 2006a; *Sorgente et al.*, 2011; *Menna et al.*, 2012]. The excess of evaporation in the Mediterranean Sea is mainly compensated by the entrance of fresh Atlantic Water (AW) through the Strait of Gibraltar. Part of this AW crosses the Sicilian channel and drives the surface circulation of the Eastern Mediterranean Sea, i.e., the Ionian and Levantine subbasins (Figure 1a). As expected for a density-driven

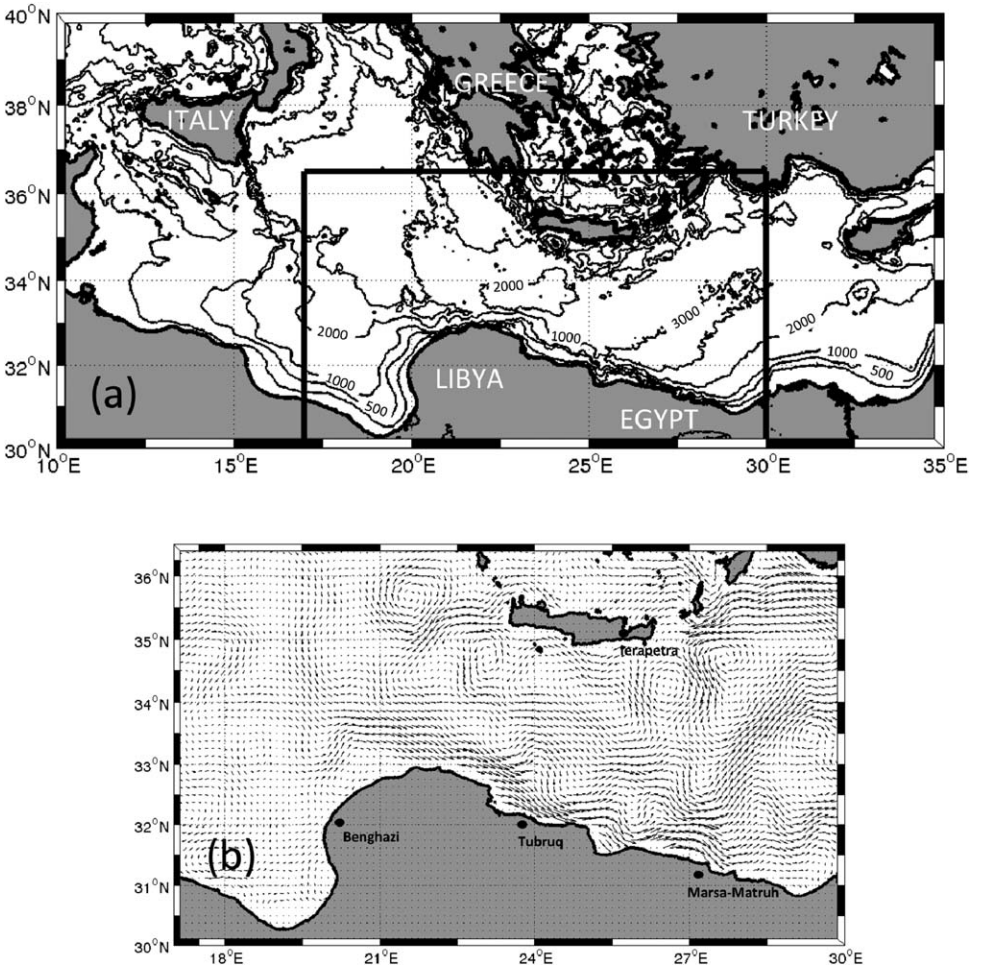

Figure 1. (a) Bathymetry of the eastern Mediterranean Sea, and (b) the 20 year average (1993–2012) of the surface geostrophic velocities computed from AVISO ADT products, in the subbasin area (17° E–30° E, 30° N–36° N).

surface current, the light AW induces a mean cyclonic circulation in the closed basin. The 20 year average of the AVISO surface geostrophic velocities (Figure 1b) exhibit a mean eastward flow along the Libyo-Egyptian coast and a mean westward flow south of Crete. However, such temporal averaging smooths out the spatio-temporal variability of coherent structures and therefore oversimplifies the basin circulation. As pointed out by *Isern-Fontanet et al*. [2006a], a large number of studies on the Mediterranean circulation are focused on mean Eulerian statistics or long-term averaged circulation [*Robinson et al*., 1991; *Larnicol et al*., 2002; *Rio et al*., 2007; *Poulain et al*., 2012; *Menna et al*., 2012] rather than on the formation and the trajectories of coherent and long-lived vortices. Indeed, the instabilities of the surface flow, the interactions with the complex bathymetry (Figure 1a), and the local wind stress generate numerous vortices in several parts of the basin. Hence, the surface circulation exhibits a strong spatiotemporal variability induced by a turbulent eddy field or highly variable currents. This is especially true in the eastern basin where the unsteady path of the AW is under debate [*Millot and Taupier-Letage*, 2005; *Gerin et al*., 2009; *Millot and Gerin*, 2010], and the mechanism of formation of coherent eddies along the Libyo-Egyptian coast poorly known. Our study focuses on the subbasin area (17° E–30° E, 30° N–36.3° N), the black rectangle in Figure 1a, where in situ measurements are scarce.

Several long-lived mesoscale features have been pointed out by observations in the eastern Mediterranean Sea [*Pinardi et al*., 2003]. Two well-documented eddies, the Ierapetra (IE) and the Pelops (PE) anticyclones, which are, respectively, located at the northwest and the southwest corners of Crete [*Theocharis et al*., 1993; *Matteoda and Glenn*, 1996], are recurrently generated in summer. Some large-scale anticyclonic gyres are visible, in these areas, on the long-term average of the surface circulation (Figure 1b). However, these eddies are not steady or permanent features even if they were observed during several months and could

sometimes survive more than a year. For instance, during the fall 1997, an old IE merged with a new IE leading to a robust anticyclonic eddy which trapped the summertime warm water in its core for almost 2 years [*Hamad et al*., 2006]. Other mesoscale anticyclones such as one Libyo-Egyptian eddies (called LE) [*Hamad et al*., 2006; *Sutyrin et al*., 2009] or the Mersa-Matruh eddies [*Hamad et al*., 2006; *Gerin et al*., 2009; *Amitai et al*., 2010; *Menna et al*., 2012] were documented from surface observations or in situ measurements in the area. However, both their lifetime and their formation areas remain unclear. Besides, the recurrent or the sporadic nature of the various mesoscale anticyclones, which are detected in this area, are still under discussion.

The main goals of this work are to identify the subregions where long-lived eddies are generated recurrently in the Eastern Mediterranean Sea, to characterize their size and intensity, and to track their trajectories. In the present paper, our study focuses on the coastal eddies (i.e., generated close to the shelf) which are able to trap and transport coastal waters in the center of the basin of the eastern Mediterranean Sea and to impact significantly the subbasin circulation in the (17°E–30°E, 30°N–36.3°N) area. We use the geostrophic velocities derived from the absolute dynamical topography of the 20 year AVISO data set covering the period 1993–2012. In order to efficiently detect and follow long-lived eddies using this relatively coarse resolution data set, we adapted and optimized the geometrical algorithm of *Nencioli et al*. [2010]. The optimized algorithm is detailed and the accuracy of our method is tested through an intercomparison of this optimized algorithm with few in situ measurements in section 2. A 20 year climatology of long-lived coastal eddies in the Eastern Mediterranean Sea is then presented in section 3. We performed here a thorough analysis of the cyclone-anticyclone asymmetry. We identify the main formation areas of long-lived eddies, we study their seasonal variability and suggest possible formation mechanisms. Finally, in section 4, we discuss these results and their impacts on the subbasin circulation.

2. Optimized Algorithm for Detection of Coastal Eddies

In order to characterize the eddy field, we choose to use the surface velocity instead of the sea surface height for several reasons. The first one is that the main dynamical properties of surface intensified vortices, namely their drifting speed [*Stegner and Zeitlin*, 1996; *Sutyrin et al*., 2009] and their stability characteristics [*Stegner and Dritschel*, 2000; *Teinturier et al*., 2010; *Lazar et al*., 2013a, 2013b], are driven by the vortex Rossby number $Ro=V_{max}/(fR_{max})$ and the Burger number $Bu=(R_d/R_{max})^2$, where V_{max} is the maximal azimuthal velocity, R_{max} the corresponding radius, R_d the internal deformation radius, and f the Coriolis parameter. Therefore, working directly with the velocities provides a direct quantification of the Rossby number Ro. Besides, in order to quantify accurately the eddy size and therefore the Burger number Bu, the radius R_{max} corresponding to the maximum tangential velocity is a simple and well-defined length. Moreover, the accurate quantification of the vortex size R_{max} and intensity V_{max} from the velocity field, provided by the AVISO data set or numerical models, will allow a direct comparison with in situ measurements such as ADCP transects or surface velocities derived from drifters trajectories.

Among the wide variety of identification methods based on the velocity field [*Sadarjoen et al*., 1998; *Isern-Fontanet et al*., 2003; *Nencioli et al*., 2010] we chose to use the approach proposed by *Nencioli et al*. [2010] which identify, for every center of rotation detected, a closed streamline corresponding to the maximal velocity ring. However, when we first applied this algorithm to the geostrophic velocities provided by AVISO (with an optimal tuning of the parameters), we were able to detect only a low number of mesoscale eddies. Hence, in order to improve the eddy detection and the eddy tracking, it was needed to significantly modify the initial algorithm. We detail below the characteristics of the data set, the main optimizations we performed on the algorithm, and the comparisons of this optimized method with in situ drifters and sea surface temperature (SST) patterns.

2.1. AVISO Geostrophic Velocities

The domain of the present study corresponds to a large fraction of the Eastern Mediterranean Sea, between the meridians of 17°E and 30°E and the parallels of 30°N and 37°N. For this region, we used the geostrophic velocity fields provided by AVISO (http://www.aviso.oceanobs.com), which are derived from the Absolute Dynamical Topography (ADT). The distributed regional product combines, for the years 1993–2012, satellite altimetry data from the Topex/Poseidon, ERS, Jason–1, and Envisat missions. This merged satellite product is projected on a 1/8° horizontal resolution Mercator grid, in time intervals of 7 days. This

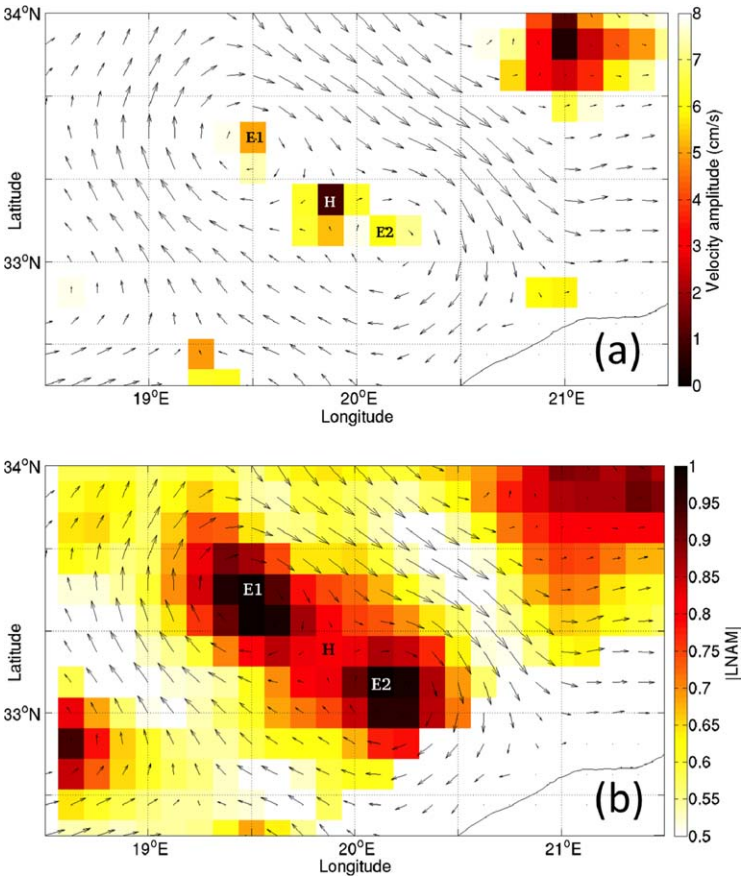

Figure 2. Example of surface geostrophic velocity fields, provided by AVSIO, with two close vortices. (a) The three grid points (H, E_1, and E_2) corresponding to local velocity minima. In this case, the lowest velocity value is found in the hyperbolic point H and not in the points E_1 or E_2, which are close to the eddy centers (elliptical points). (b) The magnitude of the *LNAM* parameter is shown for the same velocity field. In this case, the two elliptical centers (E_1 and E_2) coincides with the highest values of $|LNAM|$.

horizontal resolution is, in the Mediterranean Sea, at the order of the internal deformation radius ($R_d = 10-12$km). Hence, only large mesoscale eddies, with a typical radius R_{max} larger than the deformation radius, could be identified from this data set. Besides, the accuracy of the eddy center identification could be affected by the limited numbers of vectors in the vortex core (AVISO $1/8^\circ$ resolution).

2.2. Optimized Algorithm for the Detection of Coastal Eddies

2.2.1. Angular Momentum Method for the Detection of the Eddy Center

The first step of the method proposed by *Nencioli et al*. [2010] is to identify the centers of rotation in the velocity field. The algorithm looks for all pairs of points in the domain where there is a zonal and meridional velocity shear. At that stage, too many couples of points are selected and most of them should be excluded. Hence, the algorithm of *Nencioli et al*. [2010] searches for the local velocity minimum inside a small square domain centered on the selected points. However, the search for a velocity minimum may lead to systematic detection errors when hyperbolic and elliptic points of the velocity field are too close to each other. Such configuration is shown in Figure 2a. In this case, two vortices are next to each other and the algorithm will select the velocity minima at the hyperbolic point H of intersection between the two vortices instead of the two grid points E_1 and E_2, which are close to the vortex centers (elliptical points). Similar configuration occurs when a coastal current forms a large meander and a vortex is detached. When the current meander starts to have a closed streamline, the elliptical point (i.e., the vortex center) will also be very close to the hyperbolic point.

To correct this problem and optimize the automatic eddy detection, we totally changed the second procedure. Instead of searching for a velocity minimum, a local quantity sensitive to the velocity errors at the grid

scale, we decided to quantify an integral quantity proportional to the local angular momentum. For each grid point X_i, we quantify a Local and Normalized Angular Momentum (*LNAM*) according to the formula:

$$LNAM(X_i) = \frac{\sum_j \underline{X_i X_j} \times \underline{V_j}}{\sum_j \underline{X_i X_j} . \underline{V_j} + \sum_j |\underline{X_i X_j}||\underline{V_j}|} = \frac{L_i}{S_i + BL_i} \quad (1)$$

where X_j and $\underline{V_j}$ are, respectively, the position and the velocity vector of a grid point neighbor of X_i. The sum is made over the $n \times n$ neighbors points, inside a square domain centered on X_i. We choose here a typical size $n = 5$. This *LNAM* parameter is proportional to the local angular momentum $L_i = \sum_j \underline{X_i X_j} \times \underline{V_j}$ at the grid point X_i and it is renormalized by $BL_i = \sum_j |\underline{X_i X_j}||\underline{V_j}|$ an upper bound for the angular momentum (i.e., $-BL_i \leq L_i \leq BL_i$). Besides, we add $S_i = \sum_j \underline{X_i X_j} . \underline{V_j}$ in the renormalization term. The sum of the scalar products S_i will reach a large value for hyperbolic points and be equal to zero for elliptical points. For a symmetric vortex, if X_i is the vortex center, $S_i = 0$, and the *LNAM* parameter will reach an extremal value 1 (-1) for a cyclonic (anticyclonic) eddy. Hence, this parameter does not depend on the vortex intensity and is built to make a net distinction between hyperbolic and elliptical points. According to the Figure 2b, when this new *LNAM* parameter is used to detect the eddy centers on the same velocity field as in Figure 2a only the two elliptical points E_1 and E_2 are identified. Nevertheless, this parameter will also select the centers of current meanders even if there is no closed streamlines, in other words the extrema of the *LNAM* parameter do not guarantee a coherent eddy structure able to trap water masses in its core. Hence, we need to add a third validation step. We choose to keep the selected centers if we can find at least one closed streamline in its vicinity. The streamlines calculations are detailed below.

2.2.2. Eddy Size and Intensity

In order to define the eddy size and its intensity, we used, as *Nencioli et al*. [2010], the contours lines of the stream function field. Once the possible locations of vortex centers are identified, the local stream function is computed around each selected point. An iterative process selects an increasing set of rectangular domains until a closed streamline having the highest mean velocity V_{max} (averaged along the streamline) is found. This closed streamline is registered as the characteristic vortex contour. Inside this contour, the velocity magnitude increases radially from the vortex center. The eddy radius is then defined as the equivalent radius of a circle with the same area A as the one delimited by the closed characteristic contour:

$$R_{max} = \sqrt{\frac{A}{\pi}} \quad (2)$$

This procedure quantifies precisely for every detected eddy a characteristic size R_{max} and intensity V_{max}. Then, we can directly compute the vortex Rossby number $Ro = V_{max}/(fR_{max})$ and the Burger number $Bu = (R_d/R_{max})^2$. At that stage, we also interpolate the characteristic vortex contour by an ellipse and estimate an equivalent ellipticity $\epsilon = 1 - \frac{b}{a}$ (also called the flattening parameter) where b is the semiminor axis and a is the semimajor axis. The ellipticity of the characteristic contour could then be used to remove highly distorted structures in the statistical analysis. Moreover, we ignored eddies with a radius R_{max} smaller than 15 km. In fact, real eddies smaller than this threshold are not correctly resolved in the AVISO grid.

Figure 3 shows the 27 eddies detected by this optimized algorithm from the geostrophic velocity field (AVISO ADT data set) for the week 20–27 September 2006 in the domain under study. The eddy centers identified by the *LNAM* field are marked with a black star, and the solid lines (dashed lines) correspond to the characteristic vortex contours plotted for each anticyclones (cyclones).

The comparison with the widely used eddy detection algorithm based on the Okubo-Weiss (OW) parameter [*Isern-Fontanet et al*., 2003, 2004, 2006a; *Morrow et al*., 2004; *Chelton et al*., 2007] is given in Appendix A. The OW method, applied on the same surface velocity field, induces a strong excess of detection. More than 55 eddies were detected (Figure 18) in comparison to the 27 eddies identified with our optimized algorithm (Figure 3). This systematic over detection induced by the OW method was also highlighted in the previous studies [*Isern-Fontanet et al*., 2006a; *Chaigneau et al*., 2008; *Nencioli et al*., 2010]. Specific filters could be used to reduce the small-scale noise and the number of eddy detected [*Chelton et al*., 2007; *Souza et al*., 2011] but nevertheless, unlike the LNAM parameter we used, the OW method is highly sensitive to the variance of the flow field and therefore the threshold parameter.

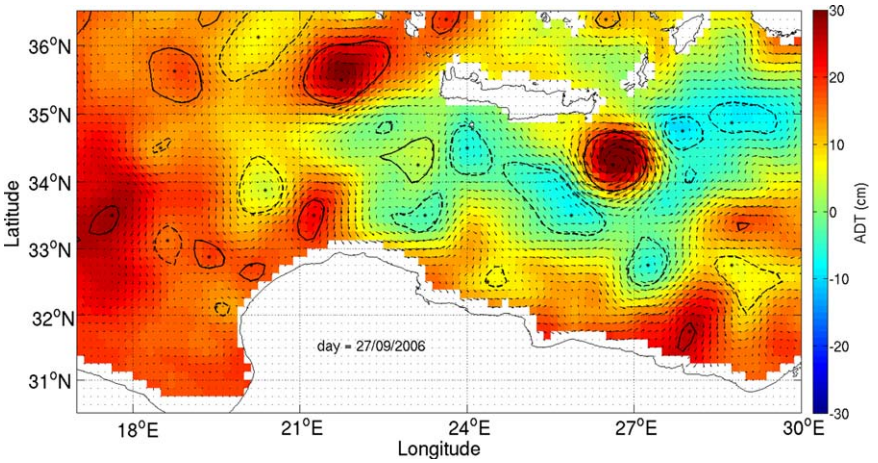

Figure 3. Eddies detected by the optimized algorithm on the AVISO geostrophic velocity field (27 September 2006) derived from the ADT altimetry data set. The black stars correspond to the eddy centers identified with the *LNAM* parameter while the solid lines (dashed lines) corresponds to the anticyclonic (cyclonic) vortex contours.

2.2.3. Eddy Tracking and Trajectory

An eddy track consists of the trajectory of an eddy during its lifetime. The method proposed for eddy tracking [*Nencioli et al*., 2010] is relatively simple and well established. Once the eddy centers are detected, eddy tracks are identified by comparing the centers at successive time steps. The trajectory of a given eddy at the week n is updated by searching the next week $n+1$ the closest eddy of the same type (cyclone/anticyclone) in a restricted area around the position of the eddy at the week n. In the present study, the radius of the search area is 45 km, in other words, the drifting speed of the eddy center cannot exceed 6.5km/d (i.e., 7.5 cms^{-1}). This value was chosen according to previous studies [*Hamad et al*., 2006; *Sutyrin et al*., 2009], which shows that typical drifting speed of mesoscale eddies in the Eastern Mediterranean Sea are around 1–3 km/d.

Vortices signature may also disappear (or be strongly smoothed) between consecutive maps, especially if their centers are located into the gaps between the satellites ground tracks. To reduce these errors, we searched for the same eddy for 2 weeks after its disappearance and increased the search area up to 67 km. Nevertheless, we cannot guarantee erroneous splitting of eddy tracks induced by measurements errors of the AVISO altimetric data set and the geostrophic velocity field derivation.

2.3. Comparison/Validation of the Optimized Method With In Situ Drifters and SST Patterns

In order to estimate the accuracy of this optimized eddy detection algorithm, we compare the trajectories, the size, and the intensity of two vortices which were sampled during the EGYPT/EGITTO program [*Taupier-Letage*, 2007]. About 100 surface velocity drifters (SVP) drogued at 15 m were released between fall 2005 and summer 2007 [*Gerin et al*., 2009]. A few of them were launched in the core of the Ierapetra anticyclone and inside one Libyo-Egyptian eddy and, where they remained trapped several months. The drifter trajectories enable to reconstruct the tracks of the eddies and to quantify their surface velocities. Besides, several CTD transects were performed at the same time across these two anticyclones. A careful comparison of eddies characteristics deduced from these in situ measurements with the ones obtained from our optimized method is detailed below. Moreover, we checked on several SST fields the agreement of the detected eddies with the SST patterns.

2.3.1. Eddies Trajectories

Among the hundred of SVP drifters launched during the EGYPT/EGITTO program, from 2005 to 2007, only a few of them got trapped inside eddies more than 2 months. Two surface drifters were trapped in the Ierapetra eddy generated in 2005 (IE05) and three other ones in the Libyo-Egyptian eddy (LE1). We use here the same notation as in *Gerin et al*. [2009] to label specific eddies. The kriging method [*Poulain and Zambianchi*, 2007] was used to filter the data set and extract the position (X_i, Y_i) and the instantaneous speed vector V_i of the drifters every 6 h. When they were trapped, the drifters looped inside the eddy with a typical period of 3–5 days. Hence, when we filter out these rapid oscillations on both the latitude and the longitude

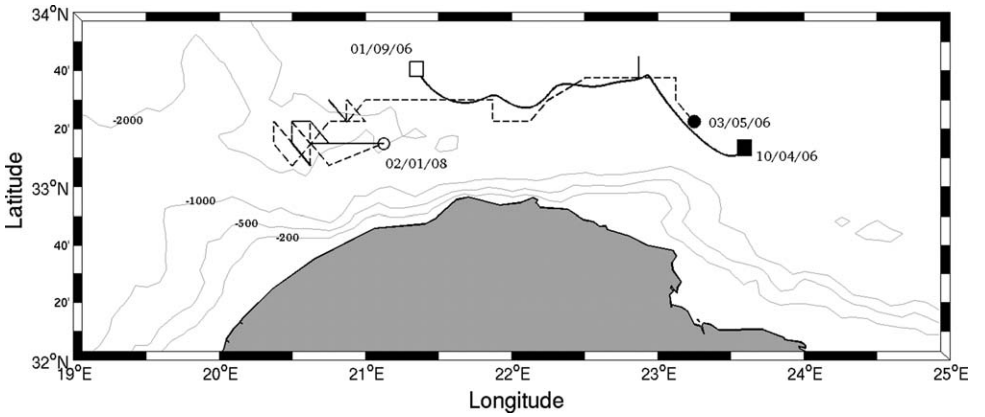

Figure 4. Trajectories of the Libyo-Egyptian eddy LE1, from April 2006 to January 2008, according to the analysis of surface drifter data set (solid line) and according to the eddy tracking algorithm applied to the AVISO data set (dashed line). The initial (final) position of the detected eddy center is plotted with a filled (open) mark. The −200, −500, −1000, and −3000 m isobaths of the shelf bathymetry are drawn (gray lines).

data set for these drifters, we can extract the slow evolution of the eddy center. The trajectory of the eddy center is then interpolated from all the trapped drifters for both anticyclones.

Among the five drifters launched in April 2006 inside the LE1 anticyclone, three drifters (b57312, b59774, and b59777) remained trapped in the eddy core for several months from April 2006 to September 2006. The westward drift of this anticyclone follows the Libyan shelf and keeps a constant distance ($L=55-65$km) between the vortex center and the 200 m bathymetry [*Sutyrin et al*., 2009], as shown in Figure 4. The trajectory deduced from the in situ drifters during this period is in very good agreement with the eddy track obtained from the AVISO data set. Even if after 6 months the surface drifters escaped from the eddy core, the automated eddy detection procedure we used allows us to follow the LE1 trajectory for 20 months. The date of the first detection of this vortex corresponds to early May 2006 when the algorithm identifies a new Libyo-Egyptian anticyclone detached from a preexisting one. According to the AVISO velocity fields, this splitting event occurred along the Libyo-Egyptian coast in late April 2006. The further evolution of the eddy is in agreement with the SST field which showed that the LE1 anticyclone (already detected in January 2006) drifted westward along the Libyan shelf for more than 1 year [*Taupier-Letage*, 2008]. We confirm here that this eddy is long lived and remains coherent for a quite long period: almost 2 years.

At the end of April 2006, four drifters were launched in the Ierapetra anticyclone IE05, two of them (b59748 and b59751) remained trapped inside the eddy core for almost 3 months until mid-July. At that time, the IE05 merged with the new Ierapetra IE06, which appeared at the end of June 2006 in the southeast corner of Crete. This merging, documented by *Taupier-Letage* [2008], is probably responsible of the ejection of the two surface drifters out of the core of IE05 in July 2006. During the 3 months period (April–July), the IE05 anticyclone slowly looped toward the North-East and the South-East (Figure 5a). As for the previous case, a very good agreement is found between the trajectories deduced, respectively, from the in situ drifters and our automated eddy tracking applied to the AVISO data set (Figure 5b). Here again, the use of the geostrophic velocity fields deduced from the ADT enables us to follow the dynamical evolution of this coherent eddy along all its lifetime: from August 2005 to September 2007. These two intercomparisons show that our optimized method provides, for large mesoscale eddies, a correct localization of the eddy center (i.e., the center of rotation) and therefore of their trajectories at the grid accuracy ($1/8^{\circ}$ for the AVISO velocity field).

2.3.2. Eddies Characteristics

When they are trapped several weeks or months inside an eddy, the in situ drifters may also provide quantitative estimations on the vortex size and its maximal velocity. Indeed, when the vortex center is accurately located we could calculate for each successive position $(X(t), Y(t))$ the radial distance $R(t)$ from the drifter to the eddy center. Specific time intervals where the drifters trajectories remain almost circular were considered: the ellipticity $\epsilon=1-b/a$ should be less than $\epsilon_0=0.3$ where b and a are, respectively, the semiminor and the semimajor axis. For all these circular loops i, we calculate the time averaged radius R_i and the mean tangential velocity V_i. Figure 6 shows the data pair (R_i, V_i) measured for both IE5 (left) and LE1 (right)

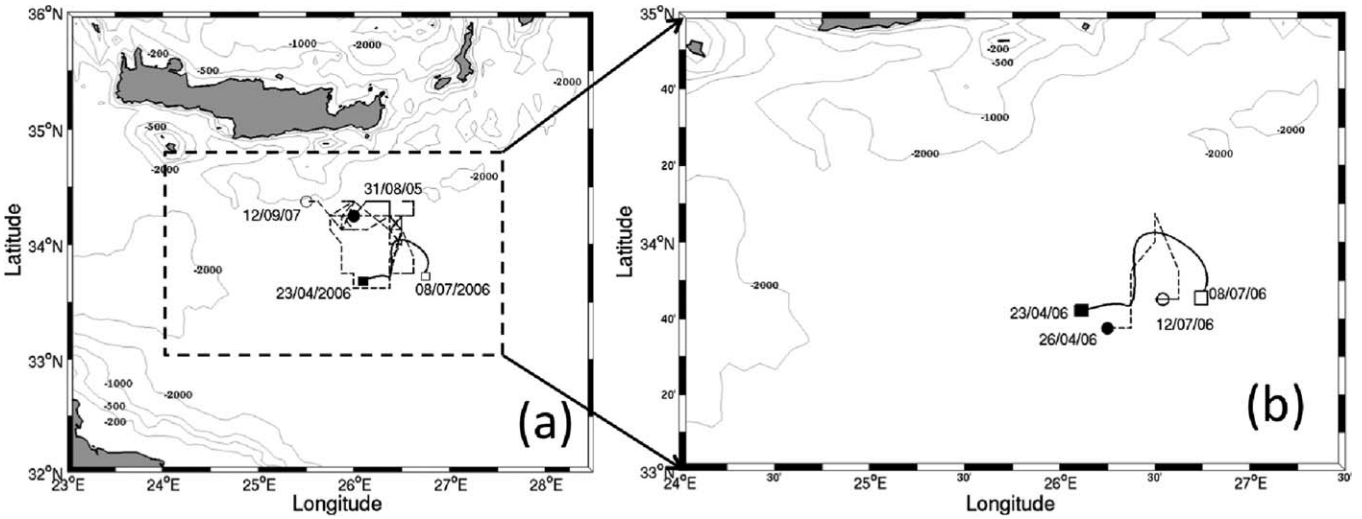

Figure 5. Trajectories of the Ierapetra eddy according to the analysis of surface drifter data set (solid line) and according to the eddy tracking algorithm applied to the AVISO data set (dashed line). The initial (final) position of the detected eddy center is plotted with a filled (open) mark. (b) The plot compares the two trajectories only during the 3 months period (April 2006 to July 2006) when surface drifters get trapped inside the eddy core.

anticyclones. The intermittency of the local wind stresses or the small-scale wave activity induces dispersion in the drifter dynamics and a wide range of R_i values are explored while the drifters loop inside the eddy. Hence, assuming that the eddy profile remains almost the same during this 3–4 months period, with only a few drifters we can estimate the core velocity profiles of these two anticyclones. As a first guess, we fit these tangential velocities with Gaussian velocity profiles (dashed lines) as a function of the radius r at each point of the eddy contour:

$$V(r) = V_{max}\frac{r}{R_{max}} exp^{(1/2 - r^2/2R_{max}^2)} \tag{3}$$

According to these in situ measurements, the maximal tangential velocities $V_{max} \simeq 35\,\mathrm{cms}^{-1}$ of the Ierapetra anticyclone is reached when $R_{max} \simeq 35\,\mathrm{km}$ while for the Libyo-Egyptian eddy, we get a larger velocity

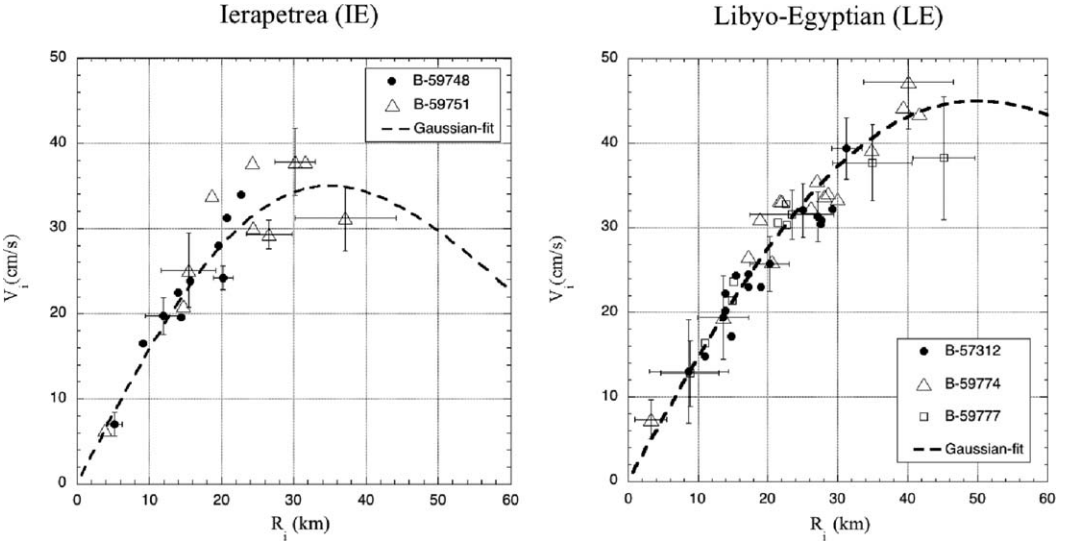

Figure 6. Mean tangential velocities V_i of the surface drifters, trapped in (left) the IE eddy or (right) the LE eddy, plotted as a function of the average radius R_i for several circular loops i. The dashed line correponds to a Gaussian profile fit according to the equation (3). The numbers B – 59748, B – 59751 correspond to the drifters ID.

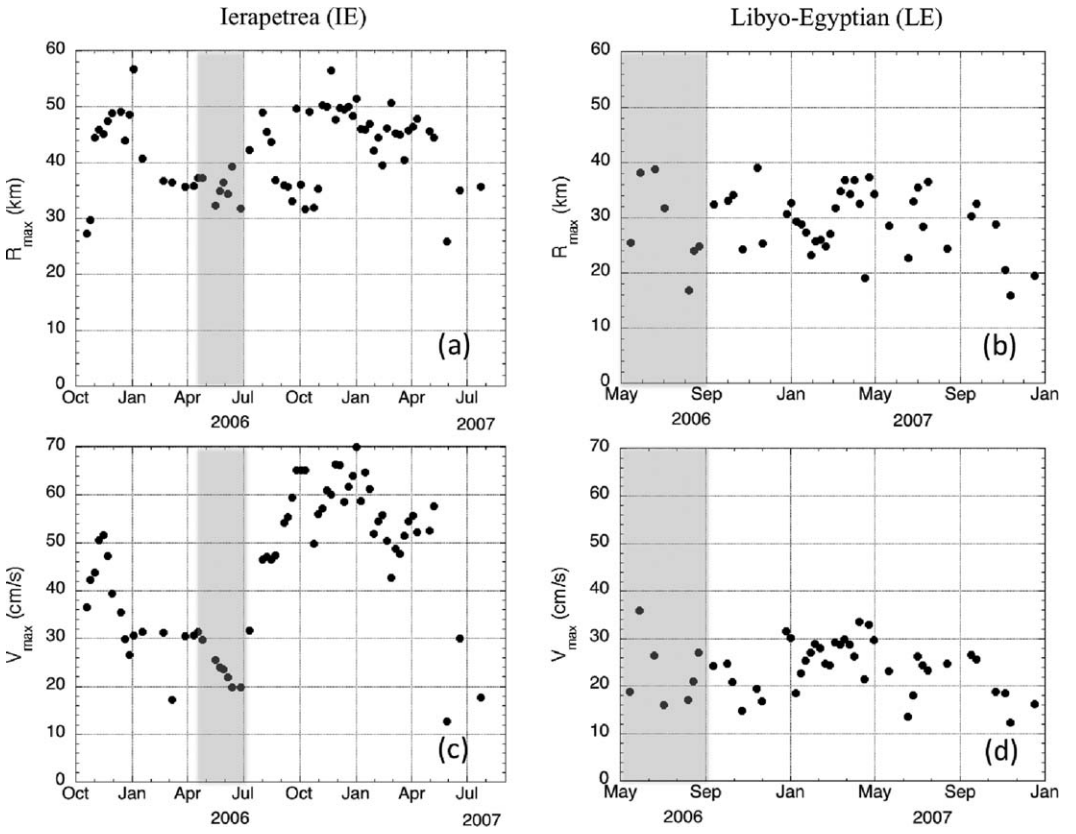

Figure 7. Temporal evolution of the radius R_{max} and the tangential velocity V_{max} of (a and c) the Ierapetra eddies and (b and d) the Libyo-Egyptian eddy according to the characteristic eddy contours given by the optimized algorithm. The gray areas represent the time period when the surface drifters were trapped inside each anticyclone.

$V_{max} \simeq 45\,\text{cm s}^{-1}$ for a larger radius $R_{max} \simeq 40-50\,\text{km}$. These typical radii are much larger than the local deformation radius $R_d = 8-12\,\text{km}$ in the area and the corresponding Burger number $Bu = (R_d/R_{max})^2$ is therefore quite small $Bu \simeq 0.04-0.08$. Then, taking into account the local Coriolis parameter f at the eddy center latitude, we can estimate the typical vortex Rossby numbers

$$Ro = \frac{V_{max}}{fR_{max}} \tag{4}$$

Even if these two anticyclones have different size and intensity they have almost the same Rossby number $Ro \simeq 0.12-0.13$. These moderate values of Ro show that the centrifugal force is relatively small in comparison with the Coriolis force and that these circular eddies comply with the geostrophic balance assumptions. Moreover, we can also estimate the core vorticity $\zeta(0)$ of these anticyclones according to the relation:

$$\zeta(r) = \partial_r V + \frac{V}{r} \tag{5}$$

For these Gaussian velocity profiles, we get

$$\left|\frac{\zeta(0)}{f}\right| = 2e^{1/2}Ro \simeq 0.4-0.43 \tag{6}$$

For such range of parameters ($Ro \simeq 0.12, \zeta(0) \simeq -0.4, Bu \simeq 0.06$), these mesoscale anticyclones cannot be affected by unstable inertial perturbations [*Kloosterziel and van Heijst*, 2006; *Carnevale et al*., 2011; *Lazar et al*., 2013a, b] and could therefore remain stable and coherent for several months.

To compare these in situ measurements to the ones obtained by the optimized algorithm applied to the AVISO data set, the temporal evolution of the typical radius R_{max} and the maximum velocity V_{max} of the characteristic eddy contours for the IE05 (left) and the LE1 (right) anticyclones are plotted in Figure 7.

Table 1. Characteristics of the Libyo-Egyptian (LE1) and the Ierapetra (IE05) Eddies[a]

	Surface Drifters	AVISO	CTD Transects
LE1 Anticyclone			
R_{max} (km)	35–45	28–32	35
V_{max} (cm/s)	45	16–28	35–45
Ro	0.12	0.06–0.14	0.12
IE05 Anticyclone			
R_{max} (km)	25–35	35	30
V_{max} (cm/s)	35	20–30	35–45
Ro	0.13	0.07–0.11	0.15

[a]The characteristic radius R_{max}, the maximal tangential velocity V_{max}, and the vortex Rossby numbers of the LE1 and the IE05 eddies are deduced from surface drifters measurements (drogued at 15 m), CTD geostrophic currents section (19–21 April 2006), and the automated eddy detection applied to the AVISO ADT geostrophic velocities.

Among the large dispersion of data, we could observe a decay of the size and the intensity of the Ierapetra eddy IE05 from the end of winter 2005 to the summer 2006. Then, the strong increase of the vortex intensity from August to October 2006 appears to be correlated to the merging of the old and weak IE05 with a new one formed and intensified by the Etesian winds during this period. The merging event was clearly visible in July 2006 from consecutive SST images [*Taupier-Letage*, 2008]. On the other hand, it is difficult to detect in the Figure 7 any seasonal fluctuations for the LE1 anticyclone, or on SST patterns [*Taupier-Letage*, 2008]. The temporal variability of the R_{max} and the V_{max} values is strong but there is no clear dynamical or meteorological reasons which could explain such variability which seems to be due either to the intrinsic errors of the remote-sensing altimetry or to the eddy detection algorithm. In order to make a relevant comparison between the automated detection algorithm and the surface drifters measurements, we consider the temporal average of the vortex size and intensities during the weeks when surface drifters were trapped inside the eddies (gray areas in Figure 7). Moreover, two CTD transects were performed during the EGYPT-1 campaign (between 19 and 21 April 2006) across the diameter of both the IE05 and the LE1 anticyclones [*Taupier-Letage et al.,* 2007; *Sutyrin et al*., 2009]. Vertical sections of the geostrophic velocities were estimated from these CTD transects, and we can then extract another independent estimation of R_{max} and V_{max} from in situ measurements. Table 1 summarizes this quantitative intercomparison. The characteristic eddy radius R_{max} of these large mesoscale eddies is correctly estimated by our optimized method. Nevertheless, we can notice that the geostrophic surface velocities, computed here from the $1/8^{\circ}$ AVISO ADT, tend to underestimate the vortex intensity even if the vortex Rossby numbers are small. Similar underestimation of the intensity of large mesoscale eddies, using the AVISO geostrophic velocities, was also observed for a wind-induced anticyclone in the wake of Madeira Island [*Caldeira et al*., 2014]. It is expected that the coarse resolution AVISO data tends to smooth down the intensity of vortices having a radius ($R_{max} = 30-40$ km) too close to the AVISO grid ($\Delta x \simeq 14$ km for the present case). According to the recent analysis of *Chelton et al*. [2011], the SSH fields of the AVISO Reference Series have been filtered to attenuate Gaussian-like features with *e*-folding radii shorter than roughly 40 km.

These two examples show that satellite altimetry provides the most useful data set to follow, with an efficient eddy tracking algorithm, the trajectories of long-lived eddies at the ocean surface. If the typical radius R_{max} of these two large mesoscale vortices are correctly estimated by the characteristic contours provided by the algorithm, their intensities V_{max} along this contour tend to be underestimated. Hence, the quantitative characterization of more intense (larger Rosby number) or smaller vortices ($R_{max} \leq 15-25$ km) from coarse gridded satellite-based measurements will be much less accurate and should be considered with care.

2.3.3. Comparison With SST Patterns

Unlike standard altimetry products, the SST or the sea color data sets could exhibit the signatures of surface oceanic structures (currents, eddies, and filaments) at high resolution. Indeed, when the wind stress is weak, the surface temperature will be advected by the surface oceanic circulation as a passive tracer. Hence, the local temperature gradients may reveal the presence of coherent structures at both meso and submesoscale due to the 1 km daily resolution of the NOAA-AVHRR SST images. Figure 8 shows the SST image taken the 18 June 2006. Among the large number of images we downloaded from the Cyprius Oceanographic Center, we selected this one because it exhibits a wide number of patterns with a high contrast. During that day and the preceding ones, the wind forcing was weak and the cloud coverage negligible in the area under study. Hence, we were able to follow the temporal evolution of the SST patterns during four consecutives days (from 16 to 19 June) and identify qualitatively the location of many cyclonic (open triangle) and anticyclonic (filled circle) circulations (Figure 8a). We consider here only the centers where a significant

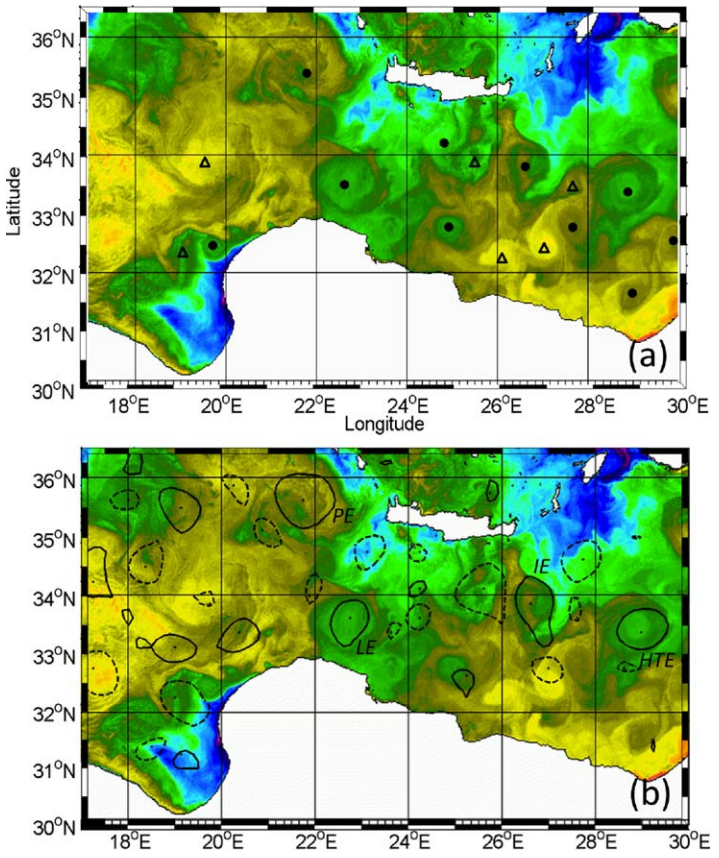

Figure 8. (a) The centers of anticylonic (filled circle) and cyclonic (triangle) motion identified on the SST field of the 18 June 2006 provided by the Cyprus Oceanographic Center. (b) The plot superimposed on the same SST field the contours of the anticyclonic (solid lines) and cyclonic (dashed lines) eddies detected by the optimized algorithm applied to the AVISO geostrophic velocity field (week 15–21, 21 June 2006).

rotation of the SST patterns was identified during the 4 days. For comparison, we superimposed in Figure 8b the same SST map and the characteristic eddy contours detected by our method applied to the geostrophic velocities provided by AVISO for the week 15–21 June 2006. We plot here all the detected eddies even those with short lifetime or with contour of high ellipticity.

We should first mention that the various patterns visible on this SST map reveal a turbulent surface circulation governed by several coherent vortices in a wide range of scales. Among this turbulent field few large-scale anticyclones, labeled IE (25.5°E, 34.25°N), PE (25.5°E, 34.25°N), LE (22.5°E, 33.75°N), and HTE (29°E, 33.5°N) in Figure 8b, are identified both from the SST patterns and from the AVISO velocities. For these four long-lived eddies, the area delimited by the characteristic contour is in correct agreement with the SST patterns even if their shape and the center locations may differ. On the other hand, the large-scale cyclonic contour (detected during several weeks in the AVISO field) located at the west of the IE05 anticyclone (Figure 8b) overestimates the size of the cyclonic SST pattern located in the same area (Figure 8a). We should mention that the SST patterns are mainly due to the Lagrangian advection of temperature gradients and therefore, there is no direct correlation with the closed contours shown in Figure 8b which correspond to instantaneous streamlines. Besides, we observe that anticyclonic (cyclonic) vortex could correspond to a cold (warm) core SST signature, due to lateral entrainment [*Taupier-Letage,* 2008]. These surprising observations confirm that the surface temperature is advected here as a passive tracer and is not correlated to the deeper thermocline structure of these geostrophic eddies. We should also note that smaller eddies, especially those along the Libyo-Egyptian coast, are not detected or correctly located by the characteristic contours we computed. This is mainly due to the limited resolution and the systematic measurements errors along the coast of altimetry data sets. These latter do not enable to resolve accurately small mesoscale vortices ($R_{max} \leq 15-25$ km) close to the coastlines or to detect submesoscale structures below the deformation radius R_d. This example clearly shows the limits of any eddy detection algorithm applied to a coarse gridded velocity field. Hence, the main limitation of our analysis comes from the $1/8^{\circ}$ resolution of the AVISO data set. Nevertheless, these few intercomparisons (even if they do not provide any statistical proofs) show that our optimized eddy detection algorithm could provide relevant detection and tracking for sufficiently large and long-lived mesoscale eddies.

3. Generations and Dynamics of Long-Lived Eddies From 1993 to 2012

We present in this section a statistical analysis of the eddies detected by the automated procedure from 1993 to 2012. We consider, in what follows, coherent structures having closed streamlines that were tracked

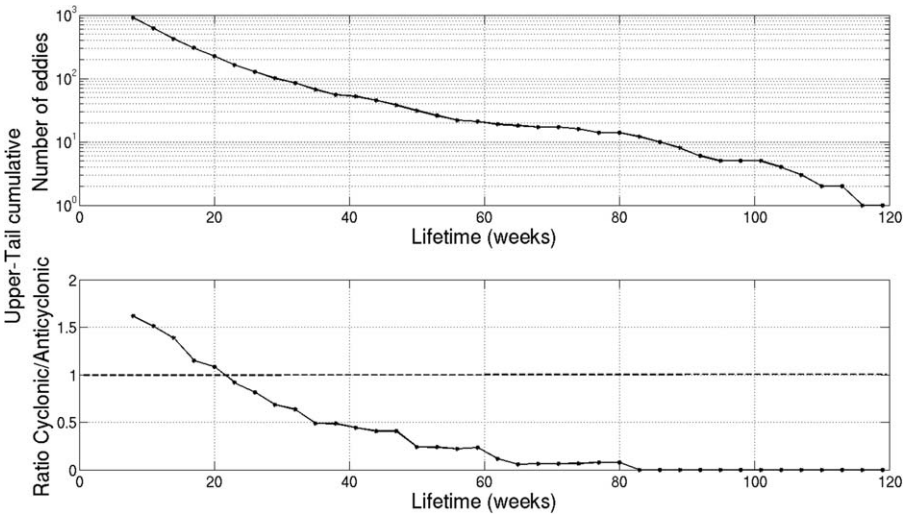

Figure 9. (top) The upper-tail cumulative histograms (the number of eddies with lifetimes greater than or equal to each particular value along the abscissa). (bottom) The upper-tail cumulative histograms of the ratio cyclones/anticyclones. Note: for instance, for eddies with lifetimes $\geq$ 8 weeks ($\geq$ 35 weeks), the ratio cyclones/anticyclones is 1.6 (0.5).

for at least 8 weeks. This minimal lifetime guarantees the coherence and the robustness of the detected structures. Among them we discarded the vortices which are, on average, too small ($R_{max} \leq 15$ km) or too elongated ($\epsilon \geq 0.3$) and we get a first list of 908 detected eddies for the 20 year period. Then, we perform a regional analysis on 270 long-lived eddies, which live more than 6 months and are able to trap and transport heat, salt, and biogeochemical species over a long distance.

3.1. Cyclone-Anticyclone Asymmetry

According to Figure 9, a large majority of the detected eddies having a lifetime that exceeds 8 weeks are cyclonic. Indeed, among these 908 eddies, 62% are cyclonic and 38% are anticyclonic. Nevertheless, this ratio is reversed if we only consider long-lived eddies. Indeed, when the lifetime exceeds 6 months the anticyclones become dominant. More than 80% of the eddies which were tracked for more than a year are anticyclonic. This dominance of anticyclones among the long-lived eddies was observed throughout most of the ocean [*Chelton et al*., 2011]. However, this asymmetry appears to be more pronounced in Eastern Mediterranean basin. According to the statistical analysis of *Chelton et al*. [2011], the dominance of anticyclones in world ocean occurs only when their lifetime exceeds 9–10 months [see *Chelton et al*., 2011, Figure 2].

Figure 10 analyses the size distribution as a function of the eddy lifetime. Large vortices ($R_{max} > 32$ km) which lived more than 21 weeks were predominantly anticyclonic while smaller eddies ($R_{max} < 32$ km) which lived shorter are mainly cyclonic (Figure 10). To explain the predominance of anticyclones among large-scale eddies, when the eddy radius becomes larger than the deformation radius, several studies were devoted to the specific stability of anticyclonic vortices in rotating shallow-water flows [*Arai and Yamagata*, 1994; *Stegner and Dritschel*, 2000; *Baey and Carton*, 2002]. Moreover, stable anticyclones tend to remain coherent within a turbulent flow [*Polvani et al*., 1994; *Arai and Yamagata*, 1994; *Linden et al*., 1995] and they were found to be more robust to external strain perturbations than cyclonic eddies [*Graves et al*., 2006]. Idealized laboratory experiments [*Perret et al*., 2006a, 2006b] and numerical simulations [*Perret et al*., 2006a, 2006b] and *Dong et al*. [2007] have shown that when the ratio of the vortex Rossby number *Ro* over the Burger number $Bu=(R_d/R_{max})^2$ becomes large, anticyclones remain coherent and circular, whereas cyclones tend to be elongated and distorted. Besides, if we take into account the weak beta effect, which may affect large-scale oceanic eddies, several studies [*Matsuura and Yamagata*, 1982; *Nycander and Sutyrin*, 1992; *Stegner and Zeitlin*, 1995, 1996] reveal that cyclonic eddies are strongly affected by the Rossby wave dispersion while anticyclones remain robust and coherent for a much longer time. Hence, the vortex stability, the nonlinear vortex-vortex interactions, and the Rossby wave dispersion all lead to the predominance of large-scale anticyclones among the long-lived eddies of the Eastern Mediterranean Sea.

3.2. Generation Areas of Long-Lived Eddies

In order to detect the formation areas of long-lived eddies along the coasts, we plot in Figure 11 the first detection points of eddies which were tracked more than 6 months during the 20 years of analysis. Once

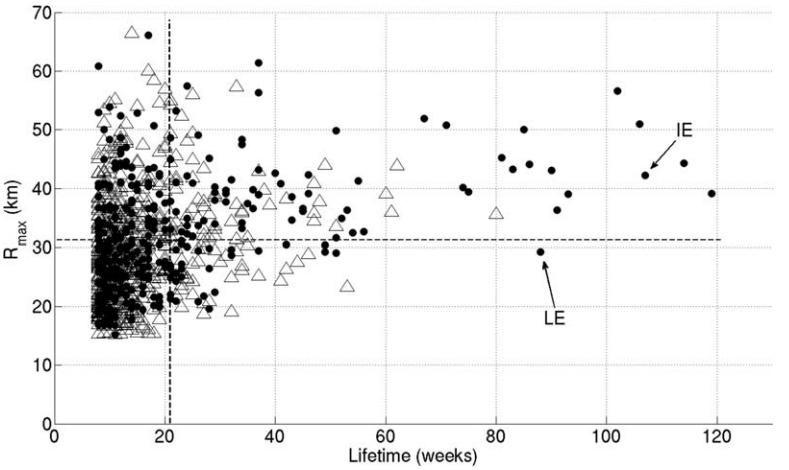

Figure 10. Mean eddy radius as a function of the eddy lifetime. The R_{max} value is here an averaged value over the whole lifetime of the eddies. Filled circle are used to represent the anticyclones while the open triangles represent the cyclones. The horizontal (vertical) dashed line corresponds to the threshold radius R_{max} =32km (threshold lifetime $\tau = 21$ weeks) where the ratio of cyclonic over anticyclonic eddies is equal to unity.

they are formed, vortices could travel a long distance, up to several hundreds of kilometers (see Figure 4), over the whole basin. If the full trajectory of all these 96 long-lived eddies were plotted, all the Eastern Mediterranean Sea would be filled by the eddy tracks. But if we plot only the initial formation points, the distribution is not uniform and specific areas could be identified. For instance, Figure 11a shows a higher density of these first detection points in the well-known areas of the Ierapetra (IE) or the Pelops (PE) eddies. The formations of large mesoscale anticyclones in these two areas were already observed and discussed in previous studies [*Hamad et al*., 2005; *Gerin et al*., 2009; *Amitai et al*., 2010; *Menna et al*., 2012]. It confirms that the first detection point computed by our tracking algorithm can identify the generation area of long-lived eddies.

Note that such a type of analysis differs from the previous ones that focused on areas of intense Eddy Kinetic Energy (EKE) [*Isern-Fontanet et al*., 2006a; *Amitai et al*., 2010; *Menna et al*., 2012]. Indeed, the kinetic energy fluctuations could be induced by the variabilities of strong currents, a large number of intense vortices having a short lifetime or by the drift of long-lived vortices which were formed elsewhere. On the other hand, the region where long-lived eddies are formed and detached regularly from the coast will necessarily be a region of strong EKE. Hence, the following analysis which focuses on the first detection points (i.e., possible generation areas) of long-lived structures will be more selective and will contain only a fraction of the intense EKE areas.

The Figure 11 clearly shows the predominance of anticyclonic vortices (59 anticyclones and 41 cyclones) and that a large majority of these mesoscale eddies tends to appear in the northern part of the basin (above 33.5°N). Only a few long-lived anticyclones are first detected in the southern part along the Libyo-Egyptian coast. If the orographic wind forcing or the instabilities of the surface current are standard mechanisms for the generation of coherent vortices we should mention that a vortex splitting that may occur in the (turbulent) open sea will lead to the formation (i.e., first detection) of a new vortex. Indeed, we observed on the high-resolution SST field few episodes of such vortex splitting in the middle of the basin. Hence, to refine the analysis and identify possible mechanisms of eddy formation, we study in the next subsection how the detection/formation points of these long-lived eddies are related to the seasonal variability.

3.3. Seasonal Variability, Possible Formation Mechanisms, and Eddies Trajectories

We plot in Figures 12 and 13 the first detection points of anticyclones and cyclones, during the 20 years of analysis, for the four seasons. We take into account the coherent eddies which were tracked more than 2 months (open circles) and the long-lived eddies that survive more than 6 months (filled circles). As in Figure 11, we can see in some specific areas a higher density of points. We focus in what follows on theses areas, delimited by dashed contours, which may correspond to formation regions for coherent and long-lived eddies.

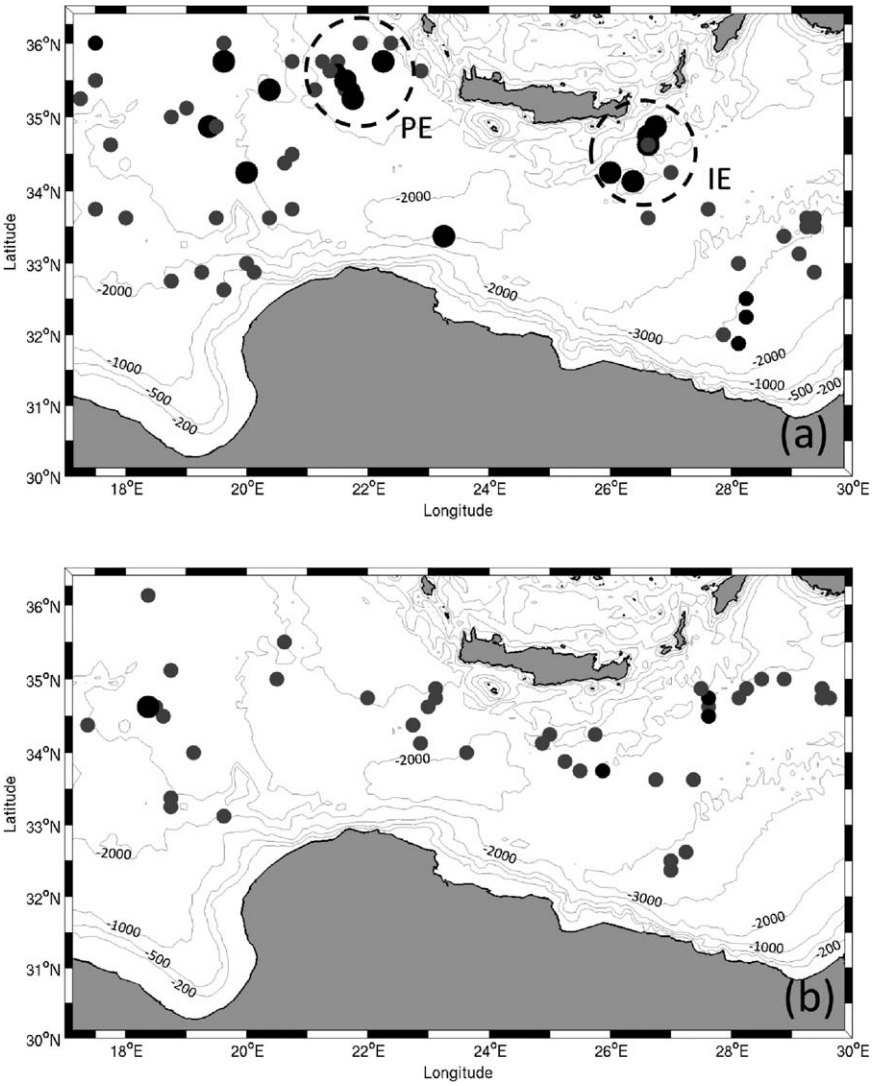

Figure 11. First detection points of long-lived (a) anticyclones and (b) cyclones during the 1993–2012 period. The dot sizes and colors correspond to the eddy lifetime: $\tau_L = 6-12$ months (small gray circle), $\tau_L = 12-18$ months (small black circle), more than 18 months (big black dots). The gray lines represent the −200, −500, −1000, −2000, and the −3000 m isobaths, respectively.

3.3.1. Ierapetra Eddies (IE)

The intense anticyclonic eddy located southeast of Crete, i.e., the Ierapetra eddy, is one of the most extensively studied vortex in this area. Several works [*Larnicol et al*., 1995; *Hamad et al*., 2006; *Amitai et al*., 2010; *Menna et al*., 2012] have observed or quantified its annual variability. The anticyclone is generated in summer, becomes fully developed in late summer or early fall and often disappears in the following spring. Figure 12 confirms that the first detection of the IE eddies occurs mainly during the summer period (21 June to 20 September). Nevertheless, in few cases, 3 among the 20 years, the formation of the Ierapetra anticyclone was not detected. Several times, it survived the whole year and merged with a new anticyclone at the summer period leading to a longer lifetime for our detection algorithm. Such a case is visible, for instance, in Figure 7c where the intensity of the IE anticyclone decayed from December 2005 to June 2006 and increased again in July 2006. The detection stops in July 2007, almost 2 years after the first detection in August 2005. A careful analysis of the eddy tracking shows that a merging event occurs, mid-July 2006, between IE05 and IE06 which emerges and grows in the southeast tip of Crete in early July 2006. These various scenarios and dynamical evolutions may explain the past discussions and controversy on the permanent or the recurrent nature of this large and intense anticyclone.

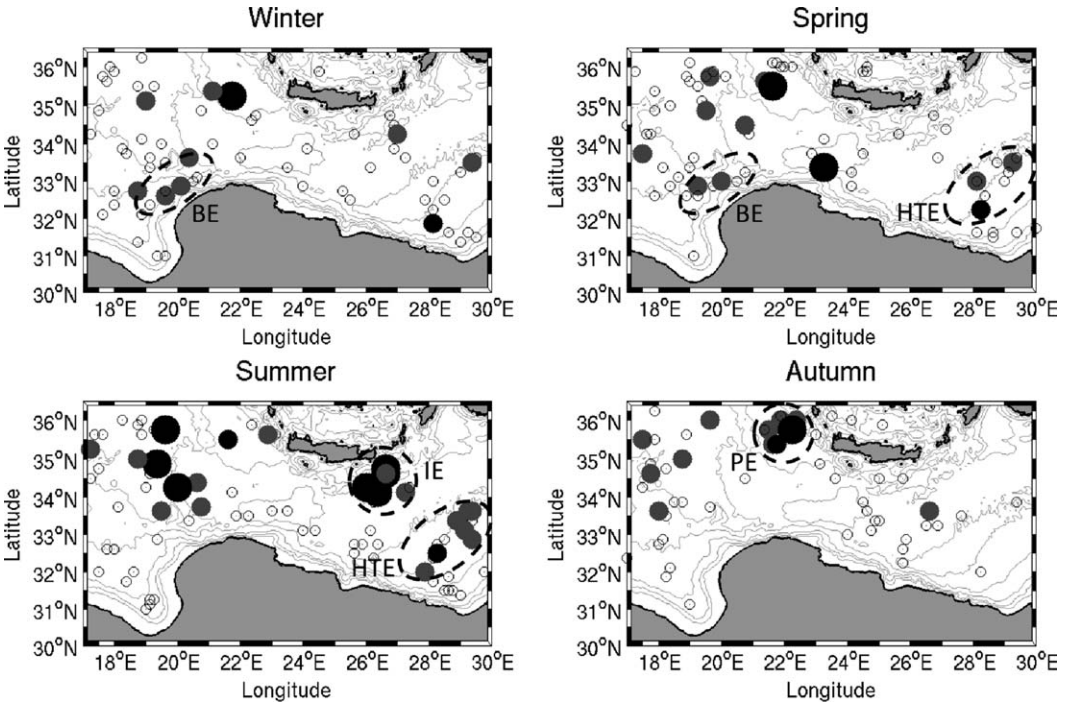

Figure 12. First detection points of long-lived anticyclones for the four seasons: (a) winter, (b) spring, (c) summer, and (d) autumn. The dot sizes and colors correspond to the eddy lifetime: τ_L=2−6 months (open circle), τ_L=6−12 months (small grey circle), τ_L=12−18 months (small black circle), more than 18 months (big black dots). The gray lines represent the −200, −500, −1000, −2000, and the −3000 m isobaths, respectively. Dashed contours indicate possible formation area.

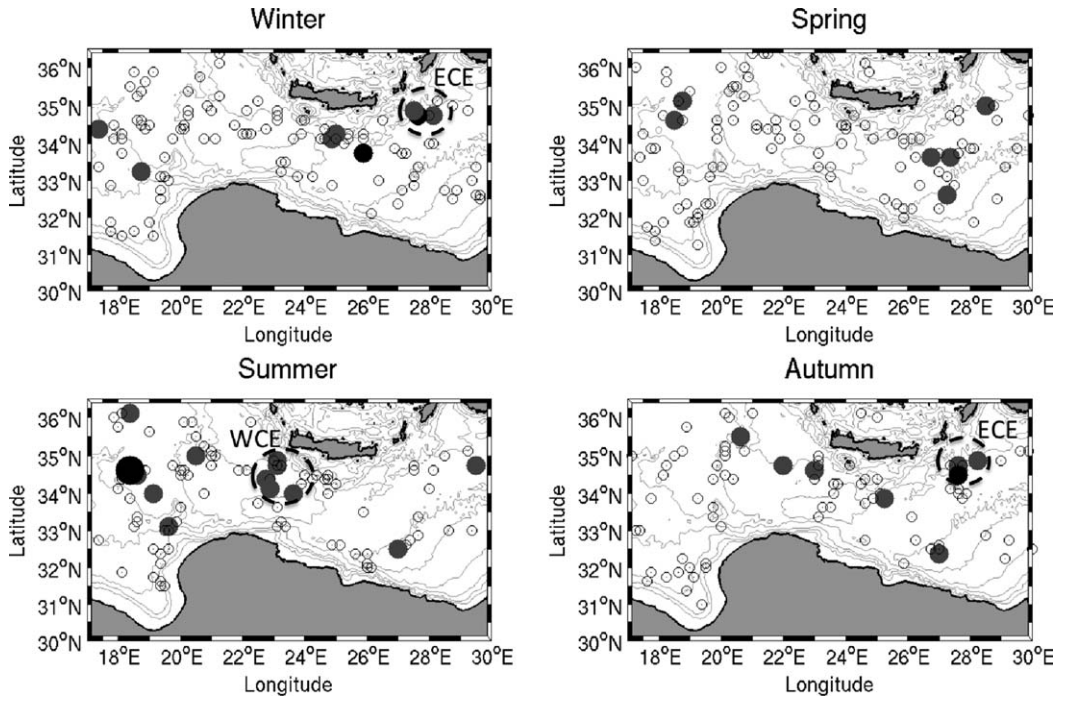

Figure 13. First detection points of long-lived cyclones for the four seasons: (a) winter, (b) spring, (c) summer, and (d) autumn. The dot sizes and colors correspond to the eddy lifetime: τ_L=2−6 months (open circle), τ_L=6−12 months (small grey circle), τ_L=12−18 months (small black circle), more than 18 months (big black dots). The gray lines represent the −200, −500, −1000, −2000, and the −3000 m isobaths, respectivley. Dashed contours indicate possible formation area.

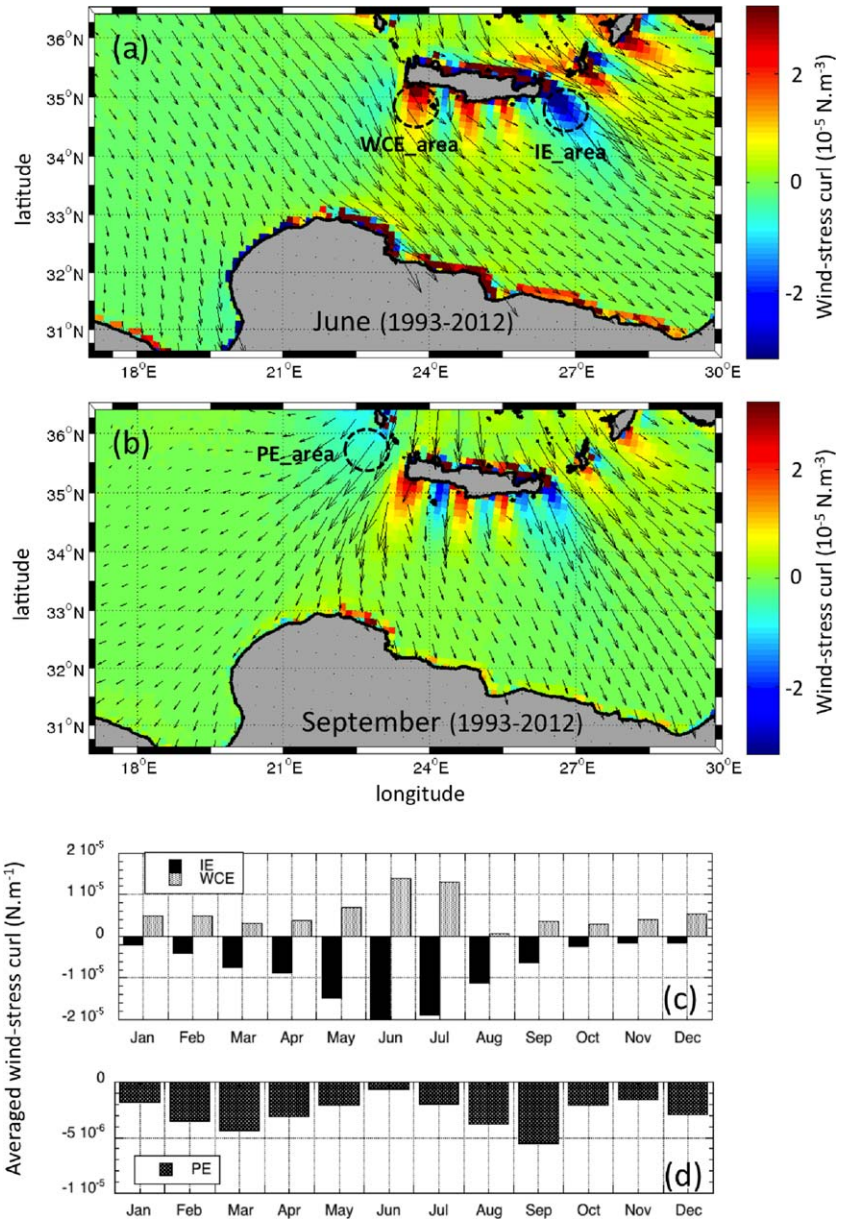

Figure 14. Wind-stress (black arrows) and wind stress-curl amplitude (colors) for the climatologic month of (a) June and (b) September. These climatologic data are averaged during the whole month for the 20 year period (1993–2012). Three areas (dashed circles labeled IE_area, PE_area, and WCE_area) were selected for the coincidence of a strong wind-stress curl with recurrent eddy formation. The seasonal cycles of the mean amplitude of the wind-stress curl, spatially averaged in each area, are plotted in (c) and (d). Note: the high pixels values visible along the coastlines are due to systematic derivative errors between the sea and the land gridded data.

The high density of first detection points during the summer period is in agreement with the *Horton et al.* [1994] hypothesis that the Ierapetra eddy is mainly forced by the Etesian winds. In order to quantify the seasonal variability of the wind forcing in the subbasin under study, we used the ALADIN data set [*Tramblay et al.*, 2013], and we compute the monthly winds climate over the 1993–2012 period. Each of these months corresponds to the arithmetic mean of the 20 monthly average wind data. We plot in Figure 14a the wind stress vectors and the wind-stress curl amplitude for the mean June which is the month having the highest wind-stress curl induced in the south of Crete by the Etesian winds. The strong wind shears found in this area are in agreement with the previous analysis of *Bakun and Agostini* [2001] and *Amitai et al.* [2010]. Moreover, we select a circular domain (IE_area in Figure 14a) centered at (26.75°E, 34.75°N) with a 45 km radius where a large number of IEs were initially detected. The Figure 14c shows that the mean wind-stress curl in

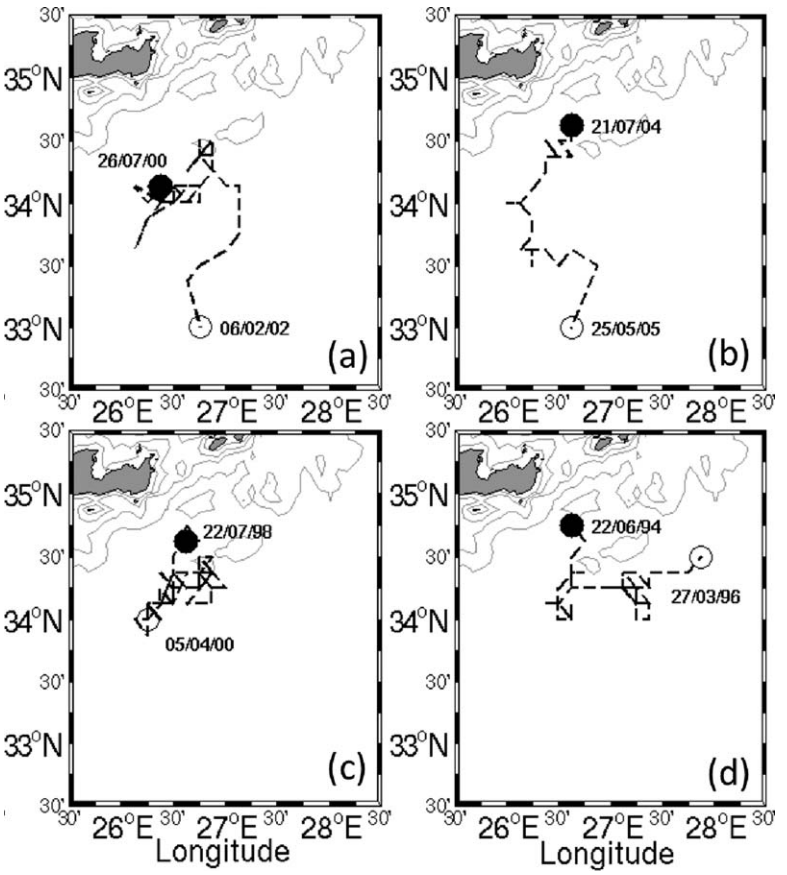

Figure 15. Trajectories of long-lived Ierapetra anticyclones (IE). The eddy trajectories (dashed lines) are plotted from the first detection point (filled circle) to the last detection point (open circle). The thin gray lines represent the −200, −500, −1000, −2000, and the −3000 m isobaths, respectively.

this IE_area starts to increase in spring and reaches its highest values in June and July. The persistence of an anticyclonic wind shear (i.e., negative wind-stress curl) is expected to induce a local Ekman downwelling and therefore favor the formation of anticyclones. Therefore, the spatial and temporal correlation between the maximum of south-east Etesian winds which occurs in late spring and early summer (Figure 14) and the first detection of the IEs in summer (Figure 12) confirms that the anticyclonic wind shear is a major forcing. The role of local wind stress as a driver for oceanic eddies was also studied in the lee of oceanic mountainous islands such as Hawai [*Calil et al*., 2008; *Jia et al*., 2011] or Madeira [*Couvelard et al*., 2012; *Caldeira et al*., 2014].

The typical radius of the detected IEs is on average ($R_{max} \simeq 35-40$ km) much larger than the local deformation radius. They are the most intense eddies in the basin with a mean Rossby number $Ro \simeq 0.15$. We plot in Figure 15 few characteristic trajectories of these IEs. Once the eddy is formed it may escape from the coast and stay relatively close to it with an irregular motion or travel toward the south. The slow southwestward drift is the most frequent trajectory (about 60%) but in a few cases we also observed a slow eastward drift.

3.3.2. Pelops Eddies (PE)

As for the Ierapetra eddy, there is a general agreement that the Pelops anticyclone (PE), located southwest of the Peloponnese [*Matteoda and Glenn*, 1996], is mainly triggered by the wind-stress curl [*Ayoub et al*., 1998]. Some authors [*Marullo et al*., 1999] also consider the meandering of the Atlantic Ionian stream (AIS) as a complementary mechanism for the generation of PEs. Our analysis exhibits, in autumn (Figure 12), a strong density of first detection points located in an area of significant anticyclonic wind-stress curl (PE_area in Figure 14). In the late summer, the Etesian winds turn from south-east (Figure 14a) to south (Figure 14b). This new direction amplifies the wind acceleration and therefore the wind shear in the Peloponnese-Cretan

strait. The monthly winds evolution in this specific area (PE_area delimited by dashed circle in Figure 14b) shows that the maximum wind-stress curl is reached in September. The previous analysis of *Bakun and Agostini* [2001] also shows that the maximum intensity of the Ekman downwelling, located in the same area, occurs in autumn, mainly in October or November according to their Figure 4f. Therefore, the fact that the PEs tends to be detected later than the IEs, is well correlated to the increases of the local wind shear in the respective formation areas. This spatiotemporal correlation gives new evidence that the wind is one of the major mechanism which drives the generation of the Pelops anticyclones.

As for the IEs, we observe from the eddy tracking algorithm that PEs may survive more than a year and merge with another anticyclone formed in the same area. Hence, many authors mention a permanent eddy [*Robinson et al*., 1991; *Theocharis et al*., 1993; *Matteoda and Glenn*, 1996] or large-scale gyre subject to seasonal variability [*Larnicol et al*., 2002].

3.3.3. Herodotus Trough Eddies (HTE)

Another area with a high concentration of first detection points is located along the Herodotus Trough (Figure 11). Surprisingly, all these points stand along the 3000 m isobath of this Mediterranean trough. A large number of mesoscale anticyclones, called Mersa-Matruh Eddies, were observed in this area [*Horton et al*., 1994; *Ayoub et al*., 1998; *Larnicol et al*., 1995; *Hamad et al*., 2006; *Amitai et al*., 2010; *Menna et al*., 2012]. Following the classification proposed by *Gerin et al*. [2009], we called eddies the Herodotus Trough Eddies (HTE) to emphasize the fact that they were initially detected along the Herodotus Trough. Several mechanisms of formation were proposed in previous studies. *Brenner* [1989] detected and surveyed a long-lived warm core eddy which appears to have formed off the coast of Egypt as a meander of the Libyo Egyptian Current (LEC). Hence, he first suggested that the coastal current instability could be the main source of HTE. According to other studies [*Robinson et al*., 1991; *Malanotte-Rizzoli and Bergamasco*, 1991; *Theocharis et al*., 1993] the "Mersa-Matruh Gyre" is a permanent feature. It was also described as a system of several eddies [*Horton et al*., 1994; *Ayoub et al*., 1998] or due to the meander of the MMJ [*Larnicol et al*., 2002].

According to our analysis of 20 years of AVISO velocity fields, the HTE seems to be mainly formed in spring and summer. We have checked that, even if the wind stress could be strong, the wind-stress curl is always negligible in this area (Figure 14). Hence, the HTE eddies cannot be wind induced and we should look for other formation mechanism. The typical trajectories of the anticyclones which were formed close to the Egyptian coast are plotted in Figure 16. All these anticyclones emerged from a coastal meander and once they escape from the coast they propagate northeastward and transport coastal waters toward the basin center, as the warm core eddy observed by *Brenner* [1989]. Hence, the instabilities of the LEC or the local changes of the mean shelf slope could explain the formation of large meanders or mesoscale eddies in this area. Some laboratory experiments have shown that when a buoyant coastal current flow from a steep to a gentle slope, the widening of the isobaths may serve as an accumulation point for the meanders generated on the steep slope [*Wolfe and Cenedese*, 2006]. On average, the typical size and vortex Rossby number of the detected HTEs were about $R_{max} = 40-45$ km and $Ro \simeq 0.1$. Nevertheless, several merging or splitting events were also observed leading to a complex eddy dynamics and a significant variability of the eddy radius. Most of the HTEs formed (i.e., first detection point) above 33°N result from the splitting of a preexisting anticyclone. A splitting event occurred in the HTE area in June 2005, according to the analyses of successive SST images (not shown). This intercomparison confirms that vortex splitting occurs (it is not an eddy detection artifact) and could be one of the recurrent mechanisms, for the formation of coherent structures in the area. Hence, the Herodotus Trough bathymetry seems to impact both the detachment point of large meanders of the LEC and the splitting of the mesoscale HTEs which travel northeastward off the Egyptian coast.

3.3.4. Benghazi Eddies (BE)

Along the Libyan coast, one area centered at 20°E, 32.5°N along the Benghazi shelf focused our attention. We noticed in this area (hereafter referred to as BE) several formation points of long-lived anticylones (Figure 12). We noticed from a thorough analysis of the geostrophic surface circulation (AVISO ADT data set) that meanders of a transient alongshore current often form in that area. The first detection points identified in the BE area correspond to the detachment of finite amplitude meanders generating mesoscale anticyclones. On average, the typical size and vortex Rossby number of the detected BEs were about $R_{max} \simeq 30-35$ km and $Ro \simeq 0.07$. The size, the intensity, and also the mean lifetime ($\tau \simeq 35$ weeks) of

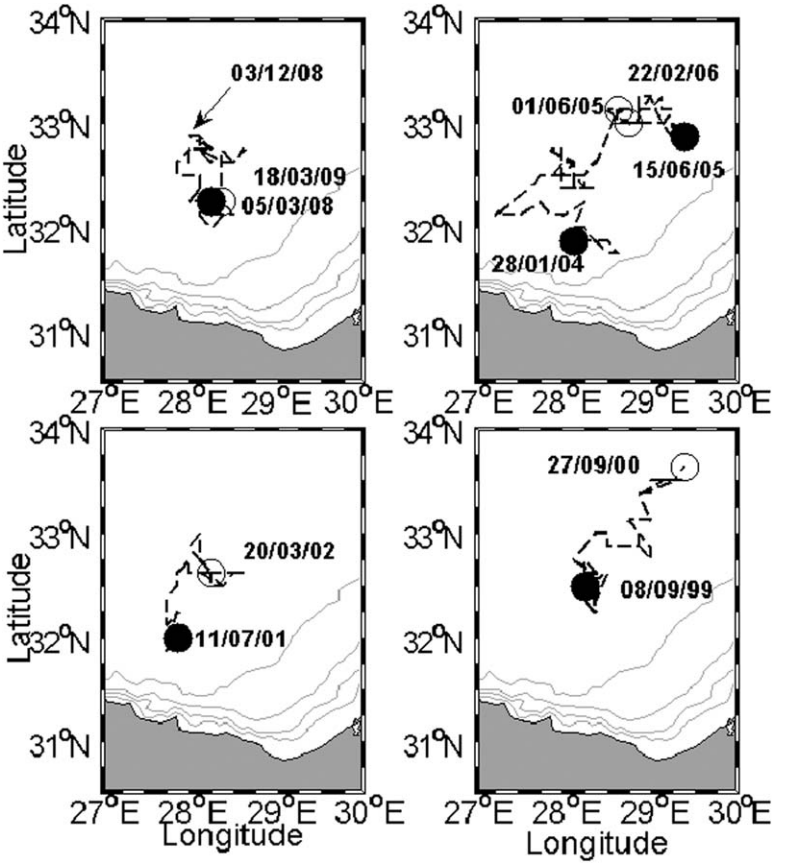

Figure 16. Trajectories of long-lived anticyclones along the Herodotus Trough. The eddy trajectories (dashed lines) are plotted from the first detection point (filled circle) to the last detection point (open circle). We add on figure (b) the "second trajectory" of the same HTE anticyclone after a strong stretching of the structure which occurs from the 1 to 15 June 2005. The thin gray lines represent the −200, −500, −1000, and the −2000 m isobaths, respectively.

the anticyclonic BEs are slightly smaller than the other large-scale anticyclones formed in the basin, especially the IEs, the PEs, and the HTEs. Their smaller size and their reduced lifetime may explain why these eddies were not discussed or identified in previous studies. The analysis of the characteristic BE trajectories shows that some eddies may stay at the same location for several months (Figures 17b and 17d). These specific events seem to indicate that the shelf bathymetry of the BE area could favor the formation or the accumulation of anticyclonic vortices. Moreover, as for the Herodotus Trough area, there is no significant and recurrent wind-stress curl along the Libyo-Egyptian coast that may trigger the formation of large-scale vortices. Hence, the formation of long-lived anticyclones in the BE area may find a plausible explanation in some instability process or the impact of the coastal bathymetry on the surface circulation.

According to Figure 17c, when a Benghazi eddy is formed slightly away from the shelf slope, this long-lived eddy propagates in the middle of the basin with an average westward drift speed of $V_d \simeq 0.4-0.45$ km/d. In order to estimate the maximum phase speed V_β of Rossby waves associated to the first baroclinic mode, we should take into account the local deformation radius $R_d = 10-12$ km. The standard Rossby wave phase speed is about $V_\beta = \beta R_d^2 \simeq 0.15-0.2$ km/d where β is the beta parameter at the eddy latitude $\theta \simeq 33^\circ$N. If we consider the westward drift of an isolated anticyclone in a reduced-gravity shallow-water model [*Nycander and Sutyrin*, 1992; *Stegner and Zeitlin*, 1995, 1996], nonlinear effects induced by the finite isopycnal deviation may lead to a supercritical drift speed of $V_d = V_\beta[1 + a(Bu/Ro)]$, where a is a geometrical factor that depends on the eddy shape. If we take $a \simeq 1$ in the first approximation, we get $V_d \simeq 0.35-0.45$ km/d when the vortex Rossby number $Ro \simeq 0.07$ and $(R_d/R_{max}) = \sqrt{Bu} \simeq 0.3$. Hence, in that case, the westward drift speed of the BEs is in good agreement with the theoretical speed of a long-lived and coherent anticyclone driven only by the beta effect.

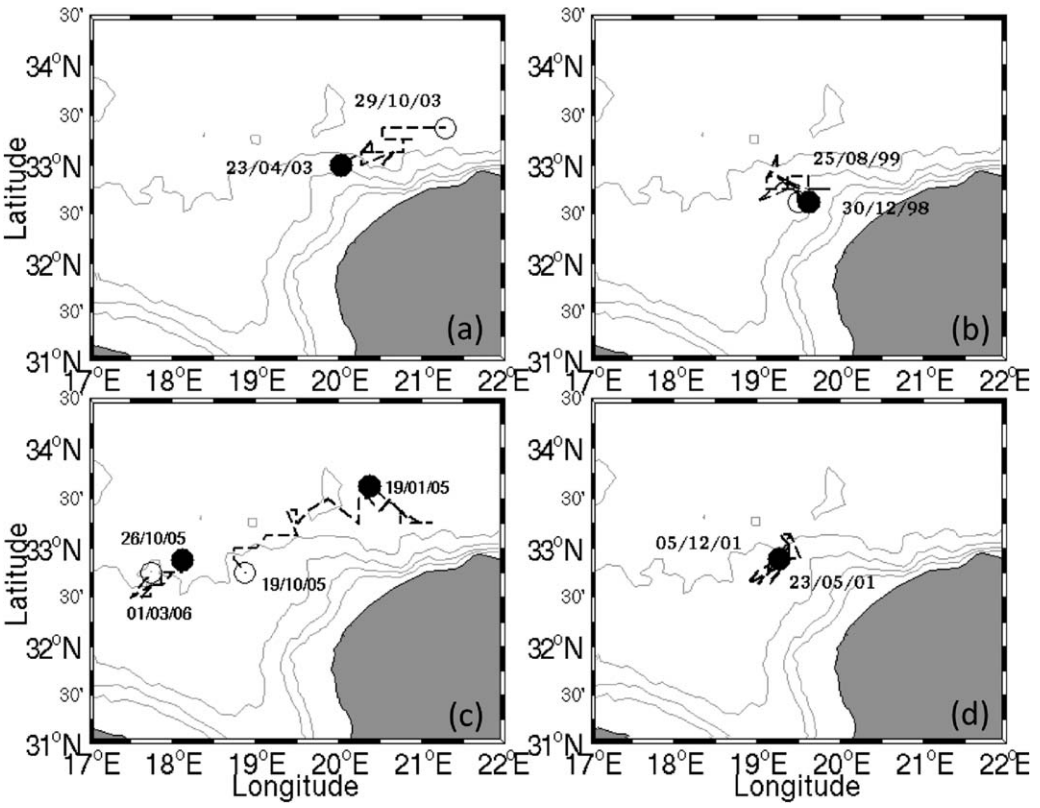

Figure 17. Trajectories of long-lived anticyclonic BE detached from the Bengahzi coast. The eddy trajectories (dashed lines) are plotted from the first detection point (filled circle) to the last detection point (open circle). We add on figure (c) the "second trajectory" of the same BE anticyclone after a strong stretching of the structure which occurs from 19 to 26 October 2005. The thin gray lines represent the −200, −500, −1000, and the −2000 m isobaths, respectively.

3.3.5. Western Cretan Eddies (WCE)

The Western Cretan Gyre, a cyclonic circulation located at the southwest of Crete, was identified in previous studies according to its SST signature and few in situ data [*Matteoda and Glenn*, 1996]. It was often described as a permanent gyre in regional circulation scheme [*Robinson et al*., 1991; *Theocharis et al*., 1993]. Figure 8 exhibits a cold SST signal in that area without any clear eddy pattern while a cyclonic eddy was detected by our analysis of the AVISO data set (the dashed contour centered at (23°E, 34.7°N) in Figure 8). The SST signature of these cold core eddies could be masked or perturbed by local warming of the sea surface layer during the summer months and it may explain the lack of detection from the SST maps. Nevertheless, according to the Figure 13, a high concentration of first detection points, labeled WCE, are detected during the summer period. The location of the WCE area coincides with the location of strong cyclonic wind-stress curl induced by the Etesian winds in June and July (Figure 14). Similar upwelling, induced by the south-east Etesian winds in the late summer, was also detected in the same area by *Bakun and Agostini* [2001]. The average size and vortex Rossby number of these cyclonic eddies are about $R_{max} \simeq 25$ km and $Ro \simeq 0.07$, which is significantly smaller and less intense than for IEs. Hence, the acceleration of the Etesian winds and the strong wind shear induced by the Cretan orography tends to generate cyclonic (the WCEs) and anticyclonic (the IEs) eddies in the near wake of this elongated island. As it is expected for large island, when the island diameter is larger than the local deformation radius [*Perret et al*., 2006b, 2010], the anticyclonic eddies are larger and more intense than the cyclonic ones for the same wake forcing.

4. Summary and Conclusions

This study provides a new statistical analysis of long-lived eddies, which stay coherent more than 6 months, in the eastern Mediterranean Sea. Unlike many other studies which tend to quantify the long-term mean circulation or the areas of intense eddy kinetic energy (EKE), we focused on the few specific areas where

long-lived eddies are generated recurrently, and we try to estimate their size, their intensity, and their characteristic trajectories from the surface geostrophic velocity fields provided by AVISO.

We first optimized the *Nencioli et al*. [2010] eddy tracking algorithm and implement a new procedure based on the computation of the Local and Normalized Angular Momentum (*LNAM*) to identify the eddy centers. This new procedure appears to be more robust and more efficient than the initial one for the analysis of coarse gridded velocity fields such as the $1/8^{\circ}$ AVISO data set. Moreover, we checked our method on two mesoscale anticyclones, the LE and the IE vortices which were sampled with several in situ drifters and CTD transects during the EGYPT campaign in 2006. We verified that our new algorithm provides a correct estimation of the eddy center and its characteristic radius R_{max} corresponding to the maximal tangential velocity V_{max}.

The analysis of 20 years of AVISO surface velocities, from 1993 to 2012, reveals a strong cyclone-anticyclone asymmetry of mesoscale vortices. The dominance of anticyclones among the long-lived eddies was observed through the statistical eddy lifetime histogram of the global ocean [*Chelton et al*., 2011] but, this study shows that this asymmetry is much more pronounced in Eastern Mediterranean Sea. We found that large vortices that lived more than 6 months were predominantly anticyclonic with a characteristic radius R_{max} exceeding by a factor two or three the local deformation radius R_d while smaller eddies lived shorter and are mainly cyclonic. The predominance of recurrent or semipermanent anticyclones in the Mediterranean Sea is often mentioned in previous studies according to various in situ observations. But, among the surface drifters which where launched and trapped several months inside eddy cores most of them were deployed inside large-scale anticyclones. This bias in the drifters deployment may have led to an overdetection of anticyclones. On the other hand, studies based on altimetric data set [*Isern-Fontanet et al*., 2006a] show a much larger number of cyclones and only a slight predominance of anticyclonic structures in the global circulation maps. Our study is the first one which quantifies precisely this asymmetry as a function of the eddy size and their lifetime. This significant predominance of long-lived and large-scale anticyclones could be explained by theoretical studies on the stability [*Arai and Yamagata*, 1994; *Stegner and Dritschel*, 2000; *Baey and Carton*, 2002] and the robustness of large-scale anticyclones on the beta plane [*Nycander and Sutyrin*, 1992; *Stegner and Zeitlin*, 1995, 1996] or in a turbulent eddy field [*Polvani et al*., 1994; *Arai and Yamagata*, 1994; *Linden et al*., 1995]. Nevertheless, this asymmetry could also be induced by the specific mechanisms of eddy generation in this area.

In order to estimate the formation areas of long-lived vortices, we provide the seasonal maps of the first detection points for both cyclones and anticyclones cumulated over the 20 years of analysis. The regions with higher density of points are considered as preferential formation areas. The spatial and temporal correlations of these specific areas with the seasonal wind-stress curl or the bottom bathymetry provides some evidences and suggest hypotheses on the various dynamical mechanisms which may govern the recurrent formation of mesoscale eddies in the eastern basin. This study confirms that the formation of both the Ierapetra and the Pelops eddies are strongly correlated to the local Ekman downwelling induced the acceleration/channeling of the Etesian winds on both side of the Cretan orography. Besides, we provide some evidence that the smaller cyclonic eddies formed at the southwest of Crete (Western Cretan Eddies) may also be induced by the same wind forcing. On the other hand, the mesoscale anticyclones formed along the Libyan or the Egyptian coasts are not directly correlated to the wind variability. We noticed that the 3000 m isobath of the Herodotus Trough seems to have a strong impact on the formation of large-scale anticyclones along and off the Mersa-Matruh coast. Besides, several eddies formed close to the coast follow this isobath and few of them split in the central basin. Hence, the strong variation of the shelf slope in this area tends to control the transport of coastal water to the open sea. Moreover, we identify a new formation area, not discussed before, along the curved shelf of the Benghazi coast. The intensity and also the mean lifetime of these anticyclonic Benghazi Eddies (BE) are slightly smaller ($R_{max} \simeq 30-35$ km) than the other mesoscale anticyclones ($R_{max} \simeq 35-40$ km) formed in the basin. If we hypothesize that these anticyclones result from the instability of a coastal current along the shelf, the steepness of the topographic slope in that area will tend to reduce the wavelength of the unstable perturbations [*Pennel et al*., 2012; *Poulin et al*., 2013] and therefore the size of coastal eddies generated from the coastal meanders. Nevertheless, in the next future, a more detailed analysis of the bathymetric impact on the coastal circulation should be done in that area to identify the possible formation mechanism.

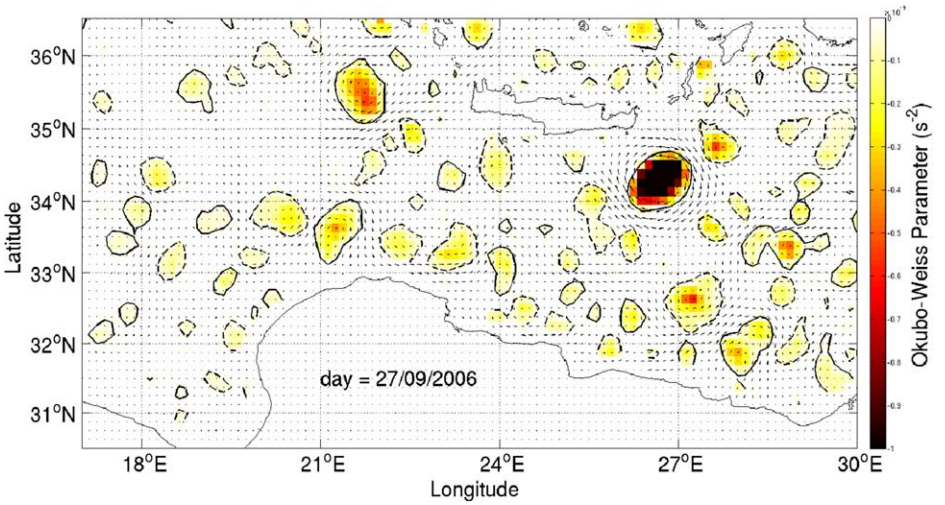

Figure 18. Same velocity field as in Figure 3. The black solid (dashed) lines correspond to the $W_0 = -0.2\sigma_\omega$ threshold of the Okubo-Weiss field around anticyclonic (cyclonic) core vortices.

Appendix A: Comparison With the Standard Okubo-Weiss Method

The Okubo-Weiss parameter $W = \sigma_n^2 + \sigma_s^2 - \zeta^2$ evaluates the relative amplitude between the local deformation and the local rotation where $\sigma_n = \frac{\partial u}{\partial x} - \frac{\partial v}{\partial y}$, $\sigma_s = \frac{\partial v}{\partial x} + \frac{\partial u}{\partial y}$, and $\zeta = \frac{\partial v}{\partial x} - \frac{\partial u}{\partial y}$ are the shearing deformation rate, the straining deformation rate, and the vertical component of vorticity, respectively. The vortex interior is dominated by vorticity and thus, negative values of W are expected in the vortex core. The pioneering work of *Isern-Fontanet et al*. [2003, 2004, 2006a] suggests to use the specific contours corresponding to the threshold $W_0 = -0.2\sigma_\omega$ to identify the vortex cores, where σ_ω is the standard deviation of the W distribution among the domain. Another study [*Chaigneau et al*., 2008] suggests that the best compromise is a W_0 value in the range $-0.3\sigma_\omega \leq W_0 \leq -0.2\sigma_\omega$.

Figure 18 shows the eddy detection using the OW method on the same surface velocity field used in Figure 3. The gray scale colorbar represents the intensity of the dimensionless W/f^2 parameter and the black solid line the standard threshold $W_0 = -0.2\sigma_\omega$. The Ierapetra (26.5°E–34.3°N) and the Pelops (21.8°E–35.6°N) eddies, are clearly identified on the Figure 18. However, in comparison with Figure 3, the OW method induces a strong excess of eddy detection. The curvature of the flow field, due to current meanders for instance, may induce a strong and localized vorticity which do not correspond to any coherent vortex with closed streamlines as detected by our optimized algorithm (Figure 3). Hence, the OW method induces a strong excess of detection.

Acknowledgments
This work was funded by the ANR-Astrid Project SYNBIOS (ANR 11 ASTR 014 01). Besides, Nadia Mkhinini thanks the national supports from DGA (Délégation Générale de l'Armement) and EDX (École Doctorale Polytechnique) in the context of the ADETOC project. We thanks Florence Sevault and Samuel Somot from CNRM/Mto-France for the atmospheric daily winds of ALADIN used in this study. Satellites data are Ssalto/Duacs Sea level anomalies and geostrophic velocity anomalies on a 1/8° regular grid over the Mediterranean Sea taken from the AVISO website: http://www.aviso.altimetry.fr/en/data/products/sea-surface-height-products/regional.html. Sea surface temperature map are taken from the Cyprus Oceanographic Center http://www.oceanography.ucy.ac.cy/cycofos/index.html. The eddy detection algorithm is available by contact to the authors.

References

Amitai, Y., Y. Lehahn, A. Lazar, and E. Heifetz (2010), Surface circulation of the eastern Mediterranean Levantine basin: Insights from analyzing 14 years of satellite altimetry data, *J. Geophys. Res.*, *115*, C10058, doi:10.1029/2010JC006147.

Arai, M., and T. Yamagata (1994), Asymmetric evolution of eddies in rotating shallow water, *Chaos*, *4*(2), 163–175, doi:10.1063/1.166001.

Ayoub, N., P.-Y. Le Traon, and P. De Mey (1998), A description of the Mediterranean surface variable circulation from combined ERS-1 and TOPEX/POSEIDON altimetric data, *J. Mar. Syst.*, *18*(1-3), 3–40, doi:10.1016/S0924-7963(98)80004-3.

Baey, J. M., and X. Carton (2002), Vortex multipoles in two-layer rotating shallow-water flows, *J. Fluid Mech.*, *460*, 151–175, doi:10.1017/S0022112002008170.

Bakun, A., and V. N. Agostini (2001), Seasonal patterns of wind-induced upwelling/downwelling in the Mediterranean Sea, *Sci. Mar.*, *65*(3), 243–257.

Brenner, S. (1989), Structure and evolution of warm core eddies in the eastern Mediterranean Levantine Basin, *J. Geophys. Res.*, *94*(C9), 12,593–12,602, doi:10.1029/JC094ic09p12593.

Caldeira, R. M. A., A. Stegner, X. Couvelard, I. B. Araújo, P. Testor, and A. Lorenzo (2014), Evolution of an oceanic anticyclone in the lee of Madeira Island: In situ and remote sensing survey, *J. Geophys. Res. Oceans*, *119*, 1195–1216, doi:10.1002/2013JC009493.

Calil, P. H. R., K. J. Richards, Y. Jia, and R. R. Bidigare (2008), Eddy activity in the lee of the Hawaiian Islands, *Deep Sea Res., Part II*, *55*(10-13), 1179–1194, doi:10.1016/j.dsr2.2008.01.008.

Carnevale, G. F., R. C. Kloosterziel, P. Orlandi, and D. D. J. A. van Sommeren (2011), Predicting the aftermath of vortex breakup in rotating flow, *J. Fluid Mech.*, *669*, 90–119, doi:10.1017/S0022112010004945.

Chaigneau, A., A. Gizolme, and C. Grados (2008), Mesoscale eddies off Peru in altimeter records: Identification algorithms and eddy spatio-temporal patterns, *Prog. Oceanogr.*, *79*(2-4), 106–119, doi:10.1016/j.pocean.2008.10.013.

Chaigneau, A., G. Eldin, and B. Dewitte (2009), Eddy activity in the four major upwelling systems from satellite altimetry (1992–2007), *Prog. Oceanogr.*, *83*(1-4), 117–123, doi:10.1016/j.pocean.2009.07.012.
Chelton, D. B., M. G. Schlax, R. M. Samelson, and R. A. de Szoeke (2007), Global observations of large oceanic eddies, *Geophys. Res. Lett.*, *34*, L15606, doi:10.1029/2007GL030812.
Chelton, D. B., M. G. Schlax, and R. M. Samelson (2011), Global observations of nonlinear mesoscale eddies, *Prog. Oceanogr.*, *91*(2), 167–216, doi:10.1016/j.pocean.2011.01.002.
Couvelard, X., R. M. A. Caldeira, I. B. Araújo, and R. Tomé (2012), Wind mediated vorticity-generation and eddy-confinement, leeward of the Madeira Island: 2008 numerical case study, *Dyn. Atmos. Oceans*, *58*, 128–149, doi:10.1016/j.dynatmoce.2012.09.005.
Dong, C., J. C. McWilliams, and A. F. Shchepetkin (2007), Island wakes in deep water, *J. Phys. Oceanogr.*, *37*(4), 962–981, doi:10.1175/JPO3047.1.
Gerin, R., P. M. Poulain, I. Taupier-Letage, C. Millot, S. B. Ismail, and C. Sammari (2009), Surface circulation in the Eastern Mediterranean using drifters (2005–2007), *Ocean Sci. Discuss.*, *6*(1), 525–555, doi:10.5194/osd-6-525-2009.
Graves, L. P., J. C. McWilliams, and M. T. Montgomery (2006), Vortex evolution due to straining: A mechanism for dominance of strong, interior anticyclones, *Geophys. Astrophys. Fluid Dyn.*, *100*(3), 151–183, doi:10.1080/03091920600792041.
Hamad, N., C. Millot, and I. Taupier-Letage (2005), A new hypothesis about the surface circulation in the eastern basin of the mediterranean sea, *Prog. Oceanogr.*, *66*(2-4), 287–298, doi:10.1016/j.pocean.2005.04.002.
Hamad, N., C. Millot, and I. Taupier-Letage (2006), The surface circulation in the eastern basin of the Mediterranean Sea, *Sci. Mar.*, *70*(3), 457–503.
Horton, C., J. Kerling, G. Athey, J. Schmitz, and M. Clifford (1994), Airborne expendable bathythermograph surveys of the eastern Mediterranean, *J. Geophys. Res.*, *99*(C5), 9891–9905, doi:10.1029/94JC00058.
Isern-Fontanet, J., E. García-Ladona, and J. Font (2003), Identification of marine eddies from altimetric maps, *J. Atmos. Oceanic Technol.*, *20*(5), 772–778, doi:10.1175/1520-0426(2003)20%3C772:iomefa%3E2.0.co;2.
Isern-Fontanet, J., J. Font, E. García-Ladona, M. Emelianov, C. Millot, and I. Taupier-Letage (2004), Spatial structure of anticyclonic eddies in the Algerian basin (Mediterranean Sea) analyzed using the Okubo-Weiss parameter, *Deep Sea Res., Part II*, *51*(25-26), 3009–3028, doi:10.1016/j.dsr2.2004.09.013.
Isern-Fontanet, J., E. García-Ladona, and J. Font (2006a), Vortices of the Mediterranean Sea: An altimetric perspective, *J. Phys. Oceanogr.*, *36*(1), 87–103, doi:10.1175/JPO2826.1.
Isern-Fontanet, J., B. Chapron, G. Lapeyre, and P. Klein (2006b), Potential use of microwave sea surface temperatures for the estimation of ocean currents, *Geophys. Res. Lett.*, *33*, L24608, doi:10.1029/2006GL027801.
Jia, Y., P. H. R. Calil, E. P. Chassignet, E. J. Metzger, J. T. Potemra, K. J. Richards, and A. J. Wallcraft (2011), Generation of mesoscale eddies in the lee of the Hawaiian Islands, *J. Geophys. Res.*, *116*, C11009, doi:10.1029/2011JC007305.
Kloosterziel, R. C., and G. J. F. van Heijst (2006), An experimental study of unstable barotropic vortices in a rotating fluid, *J. Fluid Mech.*, *223*, 1–24, doi:10.1017/S0022112091001301.
Larnicol, G., P.-Y. Le Traon, N. Ayoub, and P. De Mey (1995), Mean sea level and surface circulation variability of the Mediterranean Sea from 2 years of TOPEX/POSEIDON altimetry, *J. Geophys. Res.*, *100*(C12), 25,163–25,177, doi:10.1029/95JC01961.
Larnicol, G., N. Ayoub, and P. Y. Le Traon (2002), Major changes in Mediterranean Sea level variability from 7 years of TOPEX/Poseidon and ERS-1/2 data, *J. Mar. Syst.*, *33–34*, 63–89, doi:10.1016/S0924-7963(02)00053-2.
Lazar, A., A. Stegner, and E. Heifetz (2013a), Inertial instability of intense stratified anticyclones. Part 1. Generalized stability criterion, *J. Fluid Mech.*, *732*, 457–484, doi:10.1017/jfm.2013.412.
Lazar, A., A. Stegner, R. Caldeira, C. Dong, H. Didelle, and S. Viboud (2013b), Inertial instability of intense stratified anticyclones. Part 2. Laboratory experiments, *J. Fluid Mech.*, *732*, 485–509, doi:10.1017/jfm.2013.413.
Linden, P. F., B. M. Boubnov, and S. B. Dalziel (1995), Source-sink turbulence in a rotating stratified fluid, *J. Fluid Mech.*, *298*, 81–112, doi:10.1017/S0022112095003235.
Malanotte-Rizzoli, P., and A. Bergamasco (1991), The wind and thermally driven circulation of the eastern Mediterranean Sea. Part II: The Baroclinic case, *Dyn. Atmos. Oceans*, *15*(3-5), 355–419, doi:10.1016/0377-0265(91)90026-C.
Marullo, S., R. Santoleri, P. Malanotte-Rizzoli, and A. Bergamasco (1999), The sea surface temperature field in the Eastern Mediterranean from advanced very high resolution radiometer (AVHRR) data, *J. Mar. Syst.*, *20*(1-4), 63–81, doi:10.1016/S0924-7963(98)00071-2.
Matsuura, T., and T. Yamagata (1982), On the evolution of nonlinear planetary eddies larger than the radius of deformation, *J. Phys. Oceanogr.*, *12*(5), 440–456, doi:10.1175/1520-0485(1982)012%3C0440:oteonp%3E2.0.co;2.
Matteoda, A. M., and S. M. Glenn (1996), Observations of recurrent mesoscale eddies in the eastern Mediterranean, *J. Geophys. Res.*, *101*(C9), 20,687–20,709, doi:10.1029/96JC01111.
Menna, M., P.-M. Poulain, G. Zodiatis, and I. Gertman (2012), On the surface circulation of the Levantine sub-basin derived from Lagrangian drifters and satellite altimetry data, *Deep Sea Res., Part I*, *65*, 46–58, doi:10.1016/j.dsr.2012.02.008.
Millot, C., and R. Gerin (2010), The Mid-Mediterranean jet artefact, *Geophys. Res. Lett.*, *37*, L12602, doi:10.1029/2010GL043359.
Millot, C., and I. Taupier-Letage (2005), Circulation in the Mediterranean Sea, in *The Mediterranean Sea, Handbook of Environmental Chemistry*, vol. 5K, edited by A. Saliot, pp. 29–66, Springer, Berlin, doi:10.1007/b107143.
Morrow, R., F. Birol, D. Griffin, and J. Sudre (2004), Divergent pathways of cyclonic and anti-cyclonic ocean eddies, *Geophys. Res. Lett.*, *31*, L24311, doi:10.1029/2004GL020974.
Nencioli, F., C. Dong, T. Dickey, L. Washburn, and J. C. McWilliams (2010), A vector geometry-based eddy detection algorithm and its application to a high-resolution numerical model product and high-frequency radar surface velocities in the Southern California Bight, *J. Atmos. Oceanic Technol.*, *27*(3), 564–579, doi:10.1175/2009JTECHO725.1.
Nycander, J., and G. G. Sutyrin (1992), Steadily translating anticyclones on the beta plane, *Dyn. Atmos. Oceans*, *16*(6), 473–498, doi:10.1016/0377-0265(92)90002-B.
Pennel, R., A. Stegner, and K. Béranger (2012), Shelf impact on buoyant coastal current instabilities, *J. Phys. Oceanogr.*, *42*(1), 39–61.
Perret, G., A. Stegner, M. Farge, and T. Pichon (2006a), Cyclone-anticyclone asymmetry of large-scale wakes in the laboratory, *Phys. Fluids*, *18*(3), 036603, doi:10.1063/1.2179387.
Perret, G., A. Stegner, T. Dubos, J. M. Chomaz, and M. Farge (2006b), Stability of parallel wake flows in quasigeostrophic and frontal regimes, *Phys. Fluids*, *18*(12), 126602, doi:10.1063/1.2397563.
Perret, G., T. Dubos, and A. Stegner (2010), How Large-scale and cyclogeostrophic barotropic instabilities favor the formation of anticyclonic vortices in the ocean, *J. Phys. Oceanogr.*, *41*(2), 303–328, doi:10.1175/2010JPO4362.1.
Pinardi, N., I. Allen, E. Demirov, P. De Mey, G. Korres, A. Lascaratos, P.-Y. Le Traon, C. Maillard, G. Manzella, and C. Tziavos (2003), The mediterranean ocean forecasting system: First phase of implementation (1998–2001), *Ann. Geophys.*, *21*, 3–20.

Polvani, L. M. M., J. C. C. McWilliams, M. A. A. Spall, and R. Ford (1994), The coherent structures of shallow-water turbulence: Deformation-radius effects, cyclone/anticyclone asymmetry and gravity-wave generation, *Chaos*, *4*(2), 177–186.

Poulain, P.-M., and E. Zambianchi (2007), Surface circulation in the central Mediterranean Sea as deduced from Lagrangian drifters in the 1990s, *Cont. Shelf Res.*, *27*(7), 981–1001, doi:10.1016/j.csr.2007.01.005.

Poulain, P.-M., M. Menna, and E. Mauri (2012), Surface geostrophic circulation of the Mediterranean Sea derived from drifter and satellite altimeter data, *J. Phys. Oceanogr.*, *42*(6), 973–990, doi:10.1175/JPO-D-11-0159.1.

Poulin, F., A. Stegner, M. Hernández-Arencibia, A. Marrero-Díaz, and P. Sangrà (2013), Steep shelf stabilisation of the bransfield coastal current: Linear stability analysis, *J. Phys. Oceanogr.*, *44*, 714–732.

Rio, M. H., P. M. Poulain, A. Pascual, E. Mauri, G. Larnicol, and R. Santoleri (2007), A mean dynamic topography of the Mediterranean Sea computed from altimetric data, in-situ measurements and a general circulation model, *J. Mar. Syst.*, *65*(1-4), 484–508, doi:10.1016/j.jmarsys.2005.02.006.

Robinson, A. R., M. Golnaraghi, W. G. Leslie, A. Artegiani, A. Hecht, E. Lazzoni, A. Michelato, E. Sansone, A. Theocharis, and U. Ünlüata (1991), The eastern Mediterranean general circulation: Features, structure and variability, *Dyn. Atmos. Oceans*, *15*(3-5), 215–240, doi:10.1016/0377-0265(91)90021-7.

Sadarjoen, I. A., F. H. Post, B. Ma, D. C. Banks, and H. G. Pagendarm (1998), Selective visualization of vortices in hydrodynamic flows, in *Visualization '98 Proceedings*, pp. 419–422, IEEE, doi:10.1109/visual.1998.745333.

Sangrà, P., et al. (2009), The Canary Eddy Corridor: A major pathway for long-lived eddies in the subtropical North Atlantic, *Deep Sea Res., Part I*, *56*(12), 2100–2114, doi:10.1016/j.dsr.2009.08.008.

Schonten, M. W., W. P. M. de Ruijter, P. J. van Leeuwen, and J. R. E. Lutjeharms (2000), Translation, decay and splitting of Agulhas rings in the southeastern Atlantic Ocean, *J. Geophys. Res.*, *105*(C9), 21,913–21,925, doi:10.1029/1999JC000046.

Sorgente, R., A. Olita, P. Oddo, L. Fazioli, and A. Ribotti (2011), Numerical simulation and decomposition of kinetic energy in the central mediterranean: Insight on mesoscale circulation and energy conversion, *Ocean Sci.*, *7*(4), 503–519.

Souza, J. M. A. C., C. de Boyer Montégut, and P. Y. Le Traon (2011), Comparison between three implementations of automatic identification algorithms for the quantification and characterization of mesoscale eddies in the South Atlantic Ocean, *Ocean Sci.*, *7*(3), 317–334, doi:10.5194/os-7-317-2011.

Stegner, A., and D. G. Dritschel (2000), A numerical investigation of the stability of isolated shallow water vortices, *J. Phys. Oceanogr.*, *30*(10), 2562–2573.

Stegner, A., and V. Zeitlin (1995), What can asymptotic expansions tell us about large-scale quasi-geostrophic anticyclonic vortices?, *Nonlinear Processes Geophys.*, *2*(3/4), 186–193.

Stegner, A., and V. Zeitlin (1996), Asymptotic expansions and monopolar solitary Rossby vortices in barotropic and two-layer models, *Geophys. Astrophys. Fluid Dyn.*, *83*(3-4), 159–194, doi:10.1080/03091929608208965.

Sutyrin, G., A. Stegner, I. Taupier-Letage, and S. Teinturier (2009), Amplification of a surface-intensified eddy drift along a steep shelf in the eastern Mediterranean Sea, *J. Phys. Oceanogr.*, *39*(7), 1729–1741, doi:10.1175/2009JPO4106.1.

Taupier-Letage, I. (2008), On the use of thermal images for circulation studies: Applications to the eastern Mediterranean Basin, in *Remote Sensing of the European Seas*, edited by V. Barale and M. Gade, pp. 153–164, Springer, Netherlands, doi:10.1007/978-1-4020-6772-3_12.

Taupier-Letage, I., et al. (2007), New elements on the surface circulation in the eastern basin of the mediterranean, *Rapp. Comm. Int. Mer. Mediter.*, 38, 204.

Teinturier, S., A. Stegner, H. Didelle, and S. Viboud (2010), Small-scale instabilities of an island wake flow in a rotating shallow-water layer, *Dyn. Atmos. Oceans*, *49*(1), 1–24, doi:10.1016/j.dynatmoce.2008.10.006.

Theocharis, A., D. Georgopoulos, A. Lascaratos, and K. Nittis (1993), Water masses and circulation in the central region of the Eastern Mediterranean: Eastern Ionian, South Aegean and Northwest Levantine, 1986–1987, *Deep Sea Res., Part II*, *40*(6), 1121–1142, doi:10.1016/0967-0645(93)90064-T.

Tramblay, Y., D. Ruelland, S. Somot, R. Bouaicha, and E. Servat (2013), High-resolution med-cordex regional climate model simulations for hydrological impact studies: A first evaluation in morocco, *Hydrol. Earth Syst. Sci. Discuss.*, *10*(5), 5687–5737.

Wolfe, C. L., and C. Cenedese (2006), Laboratory experiments on eddy generation by a buoyant coastal current flowing over variable bathymetry, *J. Phys. Oceanogr.*, *36*(3), 395–411.